Physics – Uspekhi **56** (8) 747 – 771 (2013)

REVIEWS OF TOPICAL PROBLEMS PACS numbers: 05.60.Gg, **12.15. – y**, 12.60.Jv

Quantum transport and electroweak baryogenesis

T Konstandin

DOI: 10.3367/UFNe.0183.201308a.0785

Contents

Abstract. We review the mechanism of electroweak baryogenesis. Our focus is on the derivation of quantum transport equations from first principles within the Schwinger–Keldysh formalism. We emphasize the importance of the semiclassical force approach, which provides reliable predictions in most models. In light of recent electric dipole moment measurements and given the results on new physics searches from collider experiments, the status of electroweak baryogenesis is discussed in a variety of models.

1. Introduction

The goal of any baryogenesis mechanism is to explain the observed asymmetry between matter and antimatter,

$$\eta \equiv \frac{n_{\rm B} - \bar{n}_{\rm B}}{n_\gamma} \simeq 10^{-10}\,, \qquad (1)$$

where $n_{\rm B}$, $\bar{n}_{\rm B}$, and n_γ are the respective concentrations of baryons, antibaryons, and relic photons. To produce such an asymmetry dynamically, several symmetries have to be broken, which is summarized by the Sakharov conditions [1]: Baryon number (B) must not be conserved. Charge conjugation (C) and charge conjugation in combination with parity conjugation (CP) must not be a symmetry. Time reversal must not be a symmetry, which in the early Universe implies a nonequilibrium state of plasma. Owing to the Sakharov conditions, baryogenesis is only possible in extensions of the Standard Model (SM). In particular, new sources of CP violation and sizable deviation from thermal equilibrium are essential for a viable baryogenesis mechanism.

The special appeal of electroweak baryogenesis [2] (EWBG) is that only the physics of electroweak scales is involved. This makes the scenario testable in principle. The basic picture of electroweak baryogenesis is as follows: at temperatures above the electroweak scale, the electroweak gauge symmetry is unbroken and the Universe is filled with a hot plasma of particles with no net baryon number. The Universe expands and cools, and eventually the electroweak gauge symmetry is spontaneously broken via the Higgs mechanism. Electroweak baryogenesis can be realized if this change of phase proceeds by a first-order phase transition. In this case, bubbles that contain a plasma with broken electroweak symmetry nucleate and subsequently expand in the surrounding plasma with unbroken symmetry. Individual particles in the plasma experience the passing bubble interface because of their couplings to the Higgs field. This leads to the reflection of particles and drives the plasma out of equilibrium. Eventually, this reflection process entails CP violation, and an asymmetry between particles and antiparticles accumulates over time in front of the expanding bubble walls. Since the baryon number is conserved up to this point, the opposite CP asymmetry accumulates inside the bubbles of broken plasma. Finally, the baryon number is violated due to the sphaleron process, which is only active in the unbroken phase. The sphaleron also provides the C violation because it couples only to left-handed particles. This mechanism is most efficient when the particle asymmetries diffuse deep into the unbroken phase, where the sphaleron rate is unsuppressed [3]. The mechanism is sketched in Fig. 1.

T Konstandin Deutsche Elektronen Synchrotron (DESY), Notkestr. 85, 22607 Hamburg, Germany
E-mail: Thomas.Konstandin@desy.de

Received 9 October 2012
Uspekhi Fizicheskikh Nauk **183** (8) 785 – 814 (2013)
DOI: 10.3367/UFNr.0183.201308a.0785
Edited by A M Semikhatov

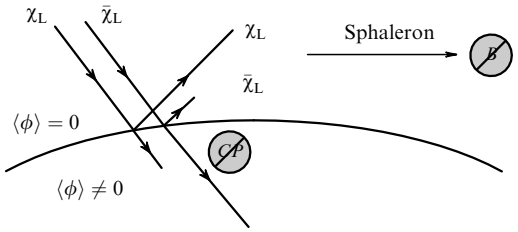

Figure 1. Sketch of the electroweak baryogenesis mechanism: Higgs bubble walls separate the symmetric from the broken phase. If the reflection of left-handed electroweak particles entails *CP* violation, the sphaleron process (which is active only in the symmetric phase) generates a net baryon number.

Among all models that provide the necessary ingredients for electroweak baryogenesis, the minimal supersymmetric standard model (MSSM) has a prominent role. This is mostly because the MSSM overcomes (or alleviates) many shortcomings of the SM in some regions of the parameter space: the hierarchy problem of the SM, unification of gauge couplings, the anomaly in the gyromagnetic moment of the muon, viable dark matter candidates, and so on. For these reasons, the MSSM is also the most studied framework for electroweak baryogenesis.

Unfortunately, electroweak baryogenesis is not so easily realized in the MSSM. The main reasons are that the Higgs sector is rather constrained and that *CP* violation arises in a special form. Even though a strong enough phase transition is possible in a small region of the parameter space (the so-called light stop scenario), the observed baryon asymmetry can only be explained by nearly mass-degenerate charginos and/or neutralinos. Therefore, a reliable analysis of the produced baryon asymmetry has to account for flavor effects, e.g., flavor oscillations, resonant enhancements, and transport phenomena that are specific to the multi-flavor case. A large part of the literature deals with these complications, which are responsible for the large discrepancies in the baryogenesis analysis among the different approaches. Recently, the available parameter space for viable MSSMs shrunk significantly with the LHC results, in particular, the Higgs searches. All in all, electroweak baryogenesis in the MSSM is technically not ruled out yet, but is only possible under rather contrived assumptions and at the cost of additional cancelations and tunings (a more detailed analysis is given in Section 4.4).

The main purpose of this review is to turn the spotlight on electroweak baryogenesis in models other than the MSSM. The emphasis is thus on the following aspects:

• With the Schwinger–Keldysh formalism [4, 5] (also see [5a]), quantum transport equations have been derived in recent years from first principles in the context of electroweak baryogenesis. Especially when the *CP* violation operative in baryogenesis results from the semiclassical force and is not based on flavor mixing, all applied approximations are well justified and allow robust quantitative predictions.

• Recent LHC results marked the discovery of a Higgs-like particle with the mass $m_h \simeq 125$ GeV. If this particle is identified with the Higgs particle, this is highly relevant for electroweak baryogenesis. The strength of the electroweak phase transition is tightly linked to the Higgs mass. Larger Higgs masses tend to weaken the phase transition and suppress the produced baryon asymmetry. In all models, we assume a Higgs mass at the above-mentioned value.

• The main motivation for new physics at the electroweak scale (and supersymmetry in particular) comes from the hierarchy problem. The discovery of the Higgs boson highlights this fact and rules out Higgsless models like Technicolor. In recent years, much progress has been made concerning alternative solutions to the hierarchy problem, such as composite Higgs models. These models typically allow electroweak baryogenesis without much tuning in the Higgs sector.

The plan of this review is as follows. In Section 2, semiclassical transport equations are derived from first principles in the Schwinger–Keldysh formalism [4, 5]. The main result in this section is Boltzmann equation (48), which includes a *CP*-violating semiclassical force at the order $\hbar$. Subsequently, in Section 3, we describe how to pass from Boltzmann-type transport equations to diffusion equations using the flow ansatz, and a complete analysis of the produced baryon asymmetry is illustrated. Finally, in Section 4, an analysis of the baryon asymmetry and its correlation with collider phenomenology is discussed in specific models. The appendices contain the remaining ingredients of the baryogenesis calculation. This includes the characteristics of the phase transition and the sphaleron rate.

2. Quantum kinetic equations

In this section, we discuss the derivation of quantum transport equations from first principles in a QFT setting and their application to electroweak baryogenesis. The main aim of this section is to sketch the Schwinger–Keldysh formalism [4, 5] (also known as the *closed time path* formalism or in-in formalism) rather than to discuss it in complete depth. The discussion closely follows the derivation in Ref. [6] and the technical review in Refs [7, 8]. More details can be found in Refs [9–11]; the thermal field theory is covered in books [12, 13].

2.1 Schwinger–Keldysh formalism

The starting point of the Schwinger–Keldysh formalism is the observation that scattering amplitudes allow not only a representation in terms of path integrals but also the time evolution of expectation values of operators [4, 5]. We consider a quantum mechanical system with coordinate q, a basis $|n\rangle$, and some operator $\hat{O}$ that at the initial time t_0 leads to the matrix elements

$$O_{mn}(t_0) = \langle m|\hat{O}|n\rangle\,. \tag{2}$$

Matrix elements evaluated at a later time can be related to $O_{mn}(t_0)$ as

$$O_{ab}(t_1) = \sum_{n,m}\langle a|\exp\left[\mathrm{i}\hat{H}(t_1-t_0)\right]|m\rangle \times O_{mn}(t_0)\langle n|\exp\left[-\mathrm{i}\hat{H}(t_1-t_0)\right]|b\rangle\,. \tag{3}$$

Hence, unlike scattering amplitudes, the time evolution of a matrix element involves the evolution of states back and forth in time.

In the path integral formulation, the evolution of the basis states can be expressed as

$$\langle n|\exp\left[-\mathrm{i}\hat{H}(t_1-t_0)\right]|b\rangle = \int \mathcal{D}q \exp\left(\mathrm{i}\int_{t_0}^{t_1}\mathrm{d}t\,\mathcal{L}(q,\dot{q})\right), \tag{4}$$

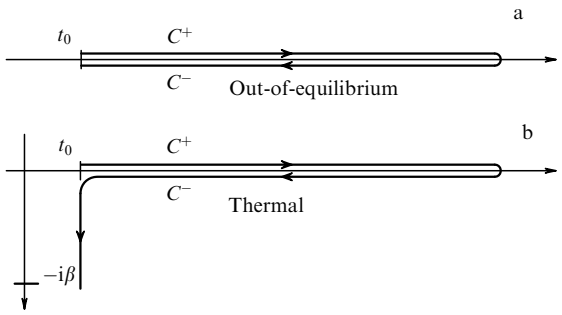

Figure 2. The closed time path contour for (a) a general out-of-equilibrium system and (b) a system in equilibrium at finite temperature.

with the Lagrangian $\mathcal{L}$ and appropriate boundary conditions. The time evolution of an operator can then be represented as

$$O_{ab}(t_1) = \int \mathcal{D}q\, O(t_1) \exp\left(\mathrm{i}\int_{\mathcal{P}} \mathrm{d}t\, \mathcal{L}(q,\dot{q})\right), \tag{5}$$

using a closed time path $\mathcal{P}$ that goes from t_0 to late times and back (see Fig. 2). It is important to remember that the two branches of integration are independent, such that in the Hamiltonian picture, operators are path ordered and not time ordered.

In QFT, the same route can be followed, leading to path integrals along a closed time path. As in the quantum mechanical example above, the evaluation of operators then leads to path-ordered expectation values. This, in turn, leads to the fact that the Dyson series of the time-dependent perturbation theory involves not only the time-ordered Green's function but also the anti-time-ordered and unordered ones. This can be expressed efficiently by giving the two-point functions an additional 2×2 structure, e.g., in the case of a scalar field ϕ, we define

$$\begin{aligned}
\Delta^{++}(u,v) &\equiv \Delta^{\mathrm{t}}(u,v) \equiv -\mathrm{i}\langle\Omega|T\left[\phi(u)\phi^{\dagger}(v)\right]|\Omega\rangle\,,\\
\Delta^{+-}(u,v) &\equiv \Delta^{<}(u,v) \equiv -\mathrm{i}\langle\Omega|\phi^{\dagger}(v)\phi(u)|\Omega\rangle\,,\\
\Delta^{-+}(u,v) &\equiv \Delta^{>}(u,v) \equiv -\mathrm{i}\langle\Omega|\phi(u)\phi^{\dagger}(v)|\Omega\rangle\,,\\
\Delta^{--}(u,v) &\equiv \Delta^{\bar{\mathrm{t}}}(u,v) \equiv -\mathrm{i}\langle\Omega|\bar{T}\left[\phi(u)\phi^{\dagger}(v)\right]|\Omega\rangle\,,
\end{aligned} \tag{6}$$

where T and $\bar{T}$ respectively denote time and anti-time ordering. Obviously, only two of the functions in (6) are independent and the matrix Δ in this $\pm$ notation is anti-Hermitian in the sense that

$$\Delta^{\dagger}(u,v) = -\Delta(v,u)\,. \tag{7}$$

In many cases, it is advantageous to express the two-point functions in terms of the spectral function $\mathcal{A} = \mathrm{i}(\Delta^{>} - \Delta^{<})/2$ and the symmetric propagator $\mathcal{F} = (\Delta^{>} + \Delta^{<})/2$. For canonically normalized fields, the spectral function satisfies the relation

$$2\partial_{u_0}\,\mathcal{A}(u,v)\Big|_{u_0\to v_0} = \delta(\mathbf{u}-\mathbf{v})\,, \tag{8}$$

which follows immediately from the equal-time commutation relations of the field ϕ.

Ultimately, matrix elements (2) can be used to determine the properties of a statistical system using the density matrix $\hat{\rho}$:

$$\mathrm{Tr}\left(\hat{\rho}\,\hat{O}\right) = \rho_{mn}O_{nm}\,. \tag{9}$$

If the density matrix is known at the initial time, the operators can be evaluated at later times using the path integral representation of O_{mn} as outlined above. In principle, all information about the system can then be inferred from the density matrix.

An alternative way to proceed is to consider a closed system of n-point functions and to impose the initial conditions on the n-point functions rather than the density matrix. In complete analogy to QFT calculations, the Schwinger–Dyson equations can be derived from the 2PI effective action [14] in the nonequilibrium setup. Formally, the equation is the same, namely,

$$\int \mathrm{d}^4w\left(\Box + m^2 + \Pi(u,w)\right)\Delta(w,v) = \delta(u-v)\,, \tag{10}$$

where Π denotes the self-energy. In a specific model, the self-energy Π can be expressed perturbatively in terms of the interactions and the two-point functions of the system. This allows determining the two-point functions at all times consistently without resorting to initial conditions in terms of a density matrix.[1]

However, even though these equations are formally the same as the Schwinger–Dyson equations, the two-point functions are understood to have the additional 2×2 structure mentioned above. Moreover, in many cases, statistical systems are not isotropic or homogeneous, and hence the two-point functions Δ and the self-energy Π depend not on the relative coordinate $u-v$ but explicitly on both coordinates u and v separately. This feature is particularly bothersome if the two-point functions are transformed into Fourier space. Usually, the Feynman calculus is particularly simple in Fourier space, since the convolutions in coordinate space turn into conventional products:

$$\int \mathrm{d}y\, A(x-y)\, B(y-z) \overset{\mathrm{FT}}{\to} A(p)\, B(p)\,. \tag{11}$$

But if a dependence on the average coordinate remains, convolutions turn into Moyal star products:

$$\int \mathrm{d}y\, A(x,y)\, B(y,z) \overset{\mathrm{FT}}{\to} A(p,X) \star B(p,X)\,. \tag{12}$$

Here, $A(p,X)$ denotes the Fourier transform with respect to the relative coordinate $r = x-y$ for a fixed central coordinate $X = (x+y)/2$:

$$A(p,X) = \int \mathrm{d}^4r\, A\left(X+\frac{r}{2},\, X-\frac{r}{2}\right)\exp(\mathrm{i}rp)\,, \tag{13}$$

and the Moyal star product is defined using the diamond operator

$$\diamond = \frac{1}{2}\left(\overleftarrow{\partial}_p\overrightarrow{\partial}_X - \overleftarrow{\partial}_X\overrightarrow{\partial}_p\right) \tag{14}$$

[1] Strictly speaking, the Schwinger–Dyson equation in the 2PI formalism allows only Gaussian initial conditions. More general initial conditions require the use of the nPI formalism or similar techniques [9, 15–18]. In the present context, this problem is not relevant because we take the limit $t_0 \to -\infty$ and hence thermal initial conditions.

by

$$A(p,X)\star B(p,X)=A(p,X)\exp\left(-\mathrm{i}\diamond\right)B(p,X)\,. \tag{15}$$

This representation of two-point functions is called the Wigner space and allows an interpretation in terms of a semiclassical phase space. One particularly simple application of this formalism is QFT at a finite temperature, which we discuss next.

2.1.1 Quantum field theory at finite temperature. The density matrix at a finite temperature is given by the Hamiltonian $\hat{H}$ and the temperature $T=\beta^{-1}$ as

$$\hat{\rho}=\exp\left(-\hat{H}\beta\right). \tag{16}$$

The partition function of this system

$$Z=\mathrm{Tr}\,\hat{\rho}=\int \mathrm{d}q\,\langle q|\exp\left(-\hat{H}\beta\right)|q\rangle \tag{17}$$

can be represented by extending the closed time path into the imaginary time direction (see Fig. 2) and imposing periodic (antiperiodic) boundary conditions for bosonic (fermionic) fields. For the two-point functions, the periodic boundary conditions turn into the Kubo–Martin–Schwinger (KMS) relation

$$\begin{aligned}&\Delta^{>}(u,v)\big|_{u_0-v_0=t}\\&\quad=\Delta^{<}(u,v)\big|_{u_0-v_0=t+\mathrm{i}\beta}\overset{\mathrm{FT}}{\to}\Delta^{>}(k)=\exp\left(k_0\beta\right)\Delta^{<}(k)\,.\end{aligned} \tag{18}$$

In combination with spectral sum rule (8),

$$\int\frac{\mathrm{d}p_0}{2\pi}\,2p_0\,\mathcal{A}(p)=1\,, \tag{19}$$

this yields

$$\begin{aligned}\mathcal{A}(p)&=\pi\delta(p^2-m^2)\,\mathrm{sign}\,(p_0)\,,\\ \mathcal{F}(p)&=-\pi\mathrm{i}\,\delta(p^2-m^2)\left(2n|\,p_0|+1\right)\end{aligned} \tag{20}$$

for a *free field* in equilibrium or, equivalently,

$$\begin{aligned}\Delta^{<}&=-\pi\mathrm{i}\delta(p^2-m^2)\,\mathrm{sign}\,(p_0)\,n(p_0)\,,\\ \Delta^{>}&=-\pi\mathrm{i}\delta(p^2-m^2)\,\mathrm{sign}\,(p_0)\left(n(p_0)+1\right).\end{aligned} \tag{21}$$

Here, we recover the Bose–Einstein particle distribution function

$$n(E)=\frac{1}{\exp\left(E\beta\right)-1}\,. \tag{22}$$

For particle species that are weakly interacting and close to equilibrium, the spectral function $\mathcal{A}$ is approximately still given by a δ-function, and the corresponding component of the plasma can be described by quasiparticles. The particle distribution function $n(X,p)$ is then encoded in the symmetric propagator $\mathcal{F}$ or the Wightman functions $\Delta^{<,>}$.

2.1.2 Kadanoff–Baym equations. It is not surprising that the Wightman functions $\Delta^{<}$ and $\Delta^{>}$ encode the particle densities in the plasma. After all, they represent the particle number operators. This indicates a way to derive quantum transport equations from first principles: Schwinger–Dyson equations (10) in Wigner space (that are also called Kadanoff–Baym (KB) equations [19]),

$$\left(p^2-m^2+\Pi(p,X)\right)\star\Delta(p,X)=1\,, \tag{23}$$

have to be solved with appropriate boundary conditions. In components, this equation can be brought to the form [7, 8]

$$\left(p^2-m^2-\Pi^{\mathrm{h}}\right)\star\Delta^{<,>}-\Pi^{<,>}\star\Delta^{\mathrm{h}}=\mathrm{coll.}, \tag{24}$$

where we introduce the collision term

$$\mathrm{coll.}=\frac{1}{2}\left(\Pi^{>}\star\Delta^{<}-\Pi^{<}\star\Delta^{>}\right), \tag{25}$$

the Hermitian part of the Green's function,

$$\Delta^{\mathrm{h}}=\Delta^{\mathrm{t}}-\frac{1}{2}(\Delta^{<}+\Delta^{>})\,, \tag{26}$$

and analogous definitions for the self-energy Π. Once the Wightman functions are known, the particle distribution functions can be obtained at later times, when the system is again close to equilibrium. According to (21), we find

$$n(X^{\mu},\mathbf{p})=4\mathrm{i}\int_{p_0>0}\frac{\mathrm{d}p_0}{2\pi}\,\Delta^{<}\,, \tag{27}$$

$$1+\bar{n}(X^{\mu},\mathbf{p})=4\mathrm{i}\int_{p_0<0}\frac{\mathrm{d}p_0}{2\pi}\,\Delta^{<}\,. \tag{28}$$

Using appropriate boundary conditions, Eqns (24) can be readily applied to the problem of electroweak baryogenesis. The system is initially close to equilibrium and driven out of equilibrium during baryogenesis. In the case of electroweak baryogenesis, this stems from the bubbles of the Higgs vacuum expectation value (vev) that give rise to a space–time-dependent mass term $m(X)$. The terms in the left-hand side describe forces that act on the particles and also the diffusion of the particle densities away from the wall. The term in the right-hand side (called the *collision term*) represents the interactions that drive the system to kinematic and chemical equilibrium. The particle densities of the species under consideration can then be obtained from the Wightman functions at later times, after the phase transition is completed.

2.2 Approximation schemes

In order to make system of equations (24) more manageable, several approximations can be applied, which we discuss in this subsection. In the context of electroweak baryogenesis, the following approximations are usually employed:[2]

• *Gradient expansion*. If the background depends only weakly on space and time coordinates, an expansion of the Moyal star products in the diamond operator can be performed. At first glance, this is a good expansion for electroweak baryogenesis, because the background only slowly varies in units of the typical momentum scale. To be specific, in the MSSM, the thickness of the Higgs bubble wall is typically $l_{\mathrm{w}}\sim 20-30\,T^{-1}$. At the same time, a typical particle in the plasma has a momentum $p\sim T$. Hence, the diamond operator reduces to a factor $\diamond\sim(l_{\mathrm{w}}T)^{-1}\ll 1$.

[2] See Ref. [20] for a similar discussion.

• *Fluid approximation*. The plasma is assumed to be close to equilibrium. In particular, it is assumed that two-to-two scatterings (or other interactions that do not change particle numbers) are fast enough, such that the plasma is well described by the local velocity of the different plasma components, the local temperatures, and the chemical potentials. The particle distribution functions can then be parameterized as

$$n \simeq \frac{1}{\exp\left[(u_\mu p^\mu + \mu)\beta\right] \pm 1}\,, \tag{29}$$

where u^μ, β, and μ are space–time dependent and denote the four-velocity, the inverse temperature, and the chemical potential of the plasma components. Taking different moments of the transport equations, we can then derive the equation of motion for these quantities (this is exemplified in Section 3).

• *Weak coupling*. Far away from the source of non-equilibrium, the system reaches its chemical equilibrium via interactions that change the particle numbers. These interactions are assumed to be slow enough for an expansion in the corresponding coupling constants to be performed.

In light of these assumptions, we can then simplify the Kadanoff–Baym equations. As a word of caution, we note that the validity of these approximations is not always guaranteed. The prime example is flavor oscillations, where the fluid approximation can fail [20]. We comment on this issue in Section 2.5.

We see shortly that the main source that drives the system out of equilibrium and induces *CP* violation arises from a kinematic effect that even persists in the limit of vanishing interactions. The deviations from equilibrium are then suppressed by $\epsilon_w \simeq (l_w T)^{-1}$, while the self-energy is suppressed by coupling constants and loop factors, $\epsilon_{\text{coll}} \simeq g^2/4\pi$. In particular, the collision term vanishes in equilibrium but also has an explicit factor ϵ_{coll} from the self-energy. Hence, we can neglect the higher gradients in the Moyal star product of the collision term and write

$$\text{coll.} \simeq \Pi^{>}(p,X)\,\Delta^{<}(p,X) - \Pi^{<}(p,X)\,\Delta^{>}(p,X)\,. \tag{30}$$

Furthermore, the terms involving the self-energy in the left-hand side of Kadanoff–Baym equation (24) mostly affect the shape of the spectral function. The term involving Π^{h} renormalizes the mass term, while the term involving $\Pi^{<,>}$ leads to a broadening of the spectral function [7, 8]. These terms are also neglected in what follows, and hence the Kadanoff–Baym equations become

$$\begin{aligned}(p^2 - m^2) \star \Delta^{<,>} \\ = \Pi^{>}(p,X)\,\Delta^{<}(p,X) - \Pi^{<}(p,X)\,\Delta^{>}(p,X)\,.\end{aligned} \tag{31}$$

2.3 One bosonic flavor

For a system with only one bosonic degree of freedom, the Wightman functions are purely imaginary, and we can immediately split the Kadanoff–Baym equations into a real part,

$$(p^2 - m^2)\cos(\diamond)\,\Delta^{<,>}(p,X) = 0\,, \tag{32}$$

and an imaginary part:

$$(p^2 - m^2)\sin(\diamond)\,\Delta^{<,>}(p,X) = \text{coll.} \tag{33}$$

The real part determines the spectral function and is usually called the *constraint equation*, while the imaginary part describes the variation of the particle distribution functions due to the background and is called the *kinetic equation*.

To the order $\mathcal{O}(\diamond^2)$, these equations are solved by the ansatz

$$\Delta^{<} = 2\pi\delta(p^2 - m^2)\,\text{sign}\,(p_0)\,n(p,X)\,, \tag{34}$$

where the particle distribution function now satisfies the equation

$$2\pi\delta(p^2 - m^2)\left(2p^\mu \partial_\mu n(p,X) + \partial_\mu m^2(X)\partial_{p_\mu} n(p,X)\right) = \text{coll.} \tag{35}$$

This equation allows a simple semiclassical interpretation. We imagine a particle with a space-dependent mass $m^2(z)$ arising from a Higgs bubble and a fixed four-momentum p^μ in front on the bubble wall. If the particle passes through the wall, its mass changes. If the semiclassical particle is on-shell on both sides of the wall, it has to change its four-momentum, and the symmetries of the problem dictate that this change arises in p_z. This reasoning leads to the relation $p_{z,\text{in}}^2 + m_{\text{in}}^2 = p_{z,\text{out}}^2 + m_{\text{out}}^2$, and the approaching particle perceives a change in mass, similarly to the case of a potential barrier. In particular, very soft particles cannot fulfill the on-shell condition inside the bubble and are reflected by the bubble wall. If this picture is generalized to a distribution of particles $n(p,X)$ and a smoothly changing mass profile $m(X)$, this leads to the statement

$$p^\mu \partial_\mu n(p,X) = -\partial_\mu m^2(X)\,\partial_{p_\mu} n(p,X)\,, \tag{36}$$

which is Eqn (35) in the absence of interactions. In the language of Boltzmann equations, the change in mass leads to a *kinematic effect* that exerts a *force* on the particles in the plasma. This effect is purely classical in the sense that it is not suppressed in the limit $\hbar \to 0$. For electroweak baryogenesis, this effect is interesting since, as we see in what follows, in the case of fermions and/or several flavors, the kinematic forces can entail *CP* violation (to the first order in $\hbar$).

Before we do so, we comment on some additional features of Eqn (35) and its solution. First, if the wall is at rest relative to the plasma, the force is absent. In the wall frame, the mass depends only on the spatial coordinates $m(z)$, while in the plasma frame, the equilibrium distribution function depends only on the energy $n(p_0)$. If these two frames coincide, the force term $\partial_\mu m^2(X)\,\partial_{p_\mu} n(p)$ vanishes, and the equilibrium solution (with the space–time-dependent mass) solves Eqn (35) everywhere. In terms of particles, soft particles are reflected, $n(\mathbf{p}) = n(-\mathbf{p})$, while hard particles replace hard particles on the other side of the bubble wall. During electroweak baryogenesis, deviations from equilibrium are hence additionally suppressed by the wall velocity v_w if it is substantially less than the speed of light.

Next, we note that the effect persists even in the limit of vanishing interactions. Once the wall is moving, the soft particles are still reflected, $n(\mathbf{p}) = n(-\mathbf{p})$, but this is not consistent with the boundary conditions of a plasma moving toward the bubble wall. Also, behind the wall, the plasma is not in equilibrium. Hence, interactions are essential to establish equilibrium far from the wall but are not so important for generating the out-of-equilibrium situation in the present context.

Finally, we note that as long as the effect from the wall can be expressed as a force,

$$p^\mu \partial_\mu n(p,X)\,\delta(p^2-m^2) = m(X)\,F_\mu(X)\,\partial_{p_\mu} n(p,X)\,\delta(p^2-m^2)\,, \tag{37}$$

the four-current

$$J^\mu = \int \mathrm{d}^4p\; p^\mu n(X,p)\,\delta(p^2-m^2) \tag{38}$$

is conserved:

$$\partial_\mu J^\mu = 0\,. \tag{39}$$

This supports the picture that the effect is kinematic and particles are neither created nor destroyed in the process. Of course, including particle-number-changing interactions from the collision term modifies this conservation law. On the other hand, the energy–momentum

$$T^{\mu\nu} = \int \mathrm{d}^4p\; p^\mu p^\nu\, n(X,p)\,\delta(p^2-m^2) \tag{40}$$

is not conserved,

$$\partial_\mu T^{\mu\nu} = \int \mathrm{d}^4p\, mF^\nu n(X,p)\,\delta(p^2-m^2) \neq 0\,, \tag{41}$$

due to the latent heat that is released during the phase transition from the Higgs sector to the plasma. But interactions preserve the (total) energy–momentum tensor

$$\int \frac{\mathrm{d}^4p}{(2\pi)^4}\, p^\mu \,\mathrm{coll.} = 0\,, \tag{42}$$

and do not modify this relation (when summed over all species). Ideally, any approximation for the transport equations that is applied subsequently should respect these laws.

2.4 One fermionic flavor

In a system with one fermionic flavor, the derivation of the Kadanoff–Baym equation parallels the bosonic case. The equation corresponding to (31) in this case yields

$$\left(\not{p} - P_\mathrm{L}\, m(X) - P_\mathrm{R}\, m^*(X)\right) \star S^<(p,X) = \mathrm{coll.}\,, \tag{43}$$

where $S^<$ denotes the fermionic Wightman function. All subleading terms are already neglected, and we introduced a complex, space–time-dependent mass. In contrast to the bosonic case, this equation cannot be simply split into constraint and kinetic equations, because the Dirac operator as well as the Green's function $S^<$ contain a spinor structure. In what follows, we assume that the change in mass is aligned with the momentum of the particle (both in the z-direction in what follows), which makes the problem effectively $(1+1)$-dimensional. If these two directions are not aligned, this situation can be achieved by a suitable Lorentz boost [21].

The spinor structure can then be partially decoupled by observing that the Dirac operator commutes with the spin operator

$$S_z = \gamma_0\gamma_3\gamma_5 \propto \gamma_1\gamma_2\,. \tag{44}$$

Using the projectors $P_s = \frac{1}{2}(\mathbf{1} + sS_z)$, the Dirac operator can be brought to a block-diagonal form. The block that encodes the vector and axial currents can then be parameterized as

$$S^< = \sum_{s=\pm} P_s S_s^<\,, \quad S_s^< = P_s\left[\gamma_0 g_0^s + \gamma_3 g_3^s + g_1^s + \gamma_5 g_2^s\right]. \tag{45}$$

In this notation, the s-even (odd) parts of g_0 encode the vector density (axial z-current), those of g_3 encode the vector z-current (axial density), and those of $g_{1/2}$ encode the scalar/pseudoscalar (z-spin densities).

In the gradient expansion, the spinor structure of the Kadanoff–Baym equations can be decoupled [6], leading to the following constraint and kinetic equations for g_0:

$$\begin{aligned} &\left(k^2 - |m|^2 - \frac{s}{k_0}\,|m|^2\theta'\right) g_0^s = 0\,,\\ &\left(k_z\partial_z - \frac{1}{2}|m^2|'\,\partial_{k_z} - \frac{s}{2k_0}\left(|m|^2\theta'\right)'\partial_{k_z}\right) g_0^s = \mathrm{coll.}, \end{aligned} \tag{46}$$

where the mass term is parameterized as $m(z) = |m(z)|\exp(\mathrm{i}\theta(z))$. Thus, the function g_0^s again allows the ansatz

$$g_0^s \propto \delta(k_0^2 - \omega_s^2) n_0^s\,, \quad \omega_s^2 \equiv k_z^2 + |m|^2 + \frac{s}{k_0}|m|^2\theta'\,, \tag{47}$$

with

$$\left(k_z\partial_z - \frac{1}{2}|m^2|'\,\partial_{k_z} - \frac{s}{2k_0}\left(|m|^2\theta'\right)'\partial_{k_z}\right) n_0^s = \mathrm{coll.} \tag{48}$$

The additional CP-violating force in this equation leads to CP-violating deviations from equilibrium in the axial z-current. The analogous equation for g_3 shows no dependence on the shift in the phase θ'. In total, no particles are produced or destroyed. Still, particles with different spins perceive different potential barriers and are reflected differently by the wall. The spin of the particles is therefore conserved, but the chirality is not.

If the wall is at rest, n_0 does not depend on k_z, and the particle distribution functions away from the wall are in their local equilibrium form. The on-shell condition is still different for particles with different spins, such that the two-point functions and the axial current J_z^5 depend on the change in the phase θ' in the wall. Since the solution is consistent with the KMS relation, including interactions does not change this picture [8]. Only if the wall velocity is nonzero can the CP violation diffuse into the symmetric phase and give rise to sizable baryogenesis.

Equation (48) is the central relation for electroweak baryogenesis with one flavor. The forces in the left-hand side of the equation encode how the plasma is driven out of equilibrium and how CP violation manifests itself in the particle densities. The kinetic term, in combination with the collision terms, dictates how the particle densities diffuse away from the wall. The collision terms also determine how the asymmetries are communicated to the other particle species and finally to the weak sphaleron. The complete electroweak baryogenesis calculation in a toy model is sketched in Section 3.

2.5 Several flavors

If several flavors are considered, additional complications arise. The diamond operator comes with a factor $\hbar$, and for one flavor, the constraint equation is algebraic in the leading order. Moreover, the kinetic equation has an overall factor $\hbar$

and is a classical transport equation in the leading order. For several flavors, the leading order of the kinetic equation (in the case of bosons) becomes

$$2k^\mu \partial_\mu \Delta^< + \mathrm{i}[m^2, \Delta^<] - \frac{1}{2}\{m^{2\prime}, \partial_{k_z}\Delta^<\} = \text{coll.} \tag{49}$$

The first two terms of this equation describe flavor oscillations with a frequency $\omega \simeq \Delta m^2/k_z \propto 1/\hbar$, while the third term gives forces similar to what was found in the one-flavor case. In the case of several flavors, the Wightman function encodes not only semiclassical particle distribution functions but also coherent superpositions of different mass eigenstates. Even though the Wightman function is diagonal in the mass eigenbasis far away from the wall, the forces induce off-diagonal entries that participate in flavor oscillations. This mechanism gives rise to new sources of *CP* violation. In particular, this effect arises already in the leading order in the kinetic equation. In comparison, the semiclassical force found for one flavor contains one more gradient (and hence one more factor $\hbar$). On the one hand, this indicates that the flavor-mixing effects can be enhanced compared with the semiclassical force. On the other hand, if the oscillation is rather fast, this suppresses the efficient population of any off-diagonal densities. Hence, it is not a priori clear if the *CP* violation stemming from mixing or the one from the semiclassical force dominates the produced baryon asymmetry.

For completeness, we quote the kinetic equation for fermions with several flavors as derived in [22] up to the second order in gradients. In this case, it is more appropriate to parameterize the two-point functions in terms of left-handed and right-handed densities. The equation for the right-handed density is given by

$$\begin{aligned} &k_z\partial_z g_\mathrm{R} + \frac{\mathrm{i}}{2}\left[m^\dagger m, g_\mathrm{R}\right] - \frac{1}{4}\left\{(m^\dagger m)', \partial_{k_z} g_\mathrm{R}\right\} \\ &\quad + \frac{1}{4k_z}\left(m^{\dagger\prime} m g_\mathrm{R} + g_\mathrm{R} m^\dagger m'\right) - \frac{1}{4k_z}\left(m^{\dagger\prime} g_\mathrm{L} m + m^\dagger g_\mathrm{L} m'\right) \\ &\quad - \frac{\mathrm{i}}{16}\left[(m^\dagger m)'', \partial_{k_z}^2 g_\mathrm{R}\right] + \frac{\mathrm{i}}{8k_z}\left[m^{\dagger\prime} m', \partial_{k_z} g_\mathrm{R}\right] \\ &\quad + \frac{\mathrm{i}}{8}\left(m^{\dagger\prime\prime} m\, \partial_{k_z}\left(\frac{g_\mathrm{R}}{k_z}\right) - \partial_{k_z}\left(\frac{g_\mathrm{R}}{k_z}\right) m^\dagger m''\right) \\ &\quad - \frac{\mathrm{i}}{8}\left(m^{\dagger\prime\prime}\, \partial_{k_z}\left(\frac{g_\mathrm{L}}{k_z}\right) m - m^\dagger\, \partial_{k_z}\left(\frac{g_\mathrm{L}}{k_z}\right) m''\right) = \text{coll.} \end{aligned} \tag{50}$$

The corresponding equation for the left-handed density is obtained by the replacements

$$g_\mathrm{R} \leftrightarrow g_\mathrm{L}\,, \quad m \leftrightarrow m^\dagger\,. \tag{51}$$

We note that this equation does not explicitly depend on the spin quantum number s, and we dropped the superscript. The dependence on s appears again when the functions are rewritten in the previous notation via

$$g_\mathrm{L}^s = g_0^s - s\, g_3^s\,, \qquad g_\mathrm{R}^s = g_0^s + s\, g_3^s\,, \tag{52}$$

and the lowest-order relation $k_z g_3 = k_0 g_0$. We also note that this kinetic equation does not explicitly depend on the energy k_0. Hence, the transport equations for particle distribution functions can be obtained by integration without knowledge of the spectral function.

The second term in (50) induces flavor oscillations, while the remaining term of first order in gradients is analogous to classical forces in the one-flavor case. These terms source the off-diagonal entries (in flavor space) of the Wightman function and contain new sources of *CP* violation, as in a bosonic system with several flavors. The last two terms reproduce the semiclassical force known from the one-flavor case.

2.5.1 Application to the MSSM. The main application of Eqn (50) is chargino (or neutralino) driven electroweak baryogenesis in the MSSM. In this framework, the semiclassical force that drives electroweak baryogenesis in the one-flavor scheme is insufficient to account for the observed baryon asymmetry. This is mainly due to a weak phase transition and rather strict constraints from EDM measurements. Hence, electroweak baryogenesis in the MSSM has to rely on flavor mixing effects that are nominally suppressed by one fewer order in the gradient expansion.

Unfortunately, some of the standard assumptions used in electroweak baryogenesis calculations potentially break down in the case of *CP* violation stemming from flavor mixing, as is discussed in detail in [20]. The oscillation frequency is $\tau_\mathrm{osc}^{-1} \sim \Delta m^2/p$, where Δm^2 denotes the difference between the mass eigenvalues squared. For soft particles, this leads to fast oscillatory behavior, and numerically this fast oscillation suppresses the relevance of the off-diagonal entries. On the other hand, flavor oscillations are important for new *CP*-violating terms that arise in kinetic equations (50) beyond the semiclassical force [22].

If the oscillations are generally assumed to be faster than the background gradients, $\tau_\mathrm{osc} \ll l_\mathrm{w}$, then the system is in the adiabatic regime [20, 23]. For the MSSM, this seems reasonable, since the bubble wall is rather thick, $l_\mathrm{w} T = 10-20$, and the charginos are never mass degenerate in the wall. Hence, the assumption that $\tau_\mathrm{osc} \ll l_\mathrm{w}$ should be valid for a typical particle in a plasma with $p \sim T$. In this regime, flow ansatz (29) (including a collective oscillation) seems reasonable. Furthermore, back reactions from the off-diagonal densities on the diagonal ones are small[3] and can be neglected. This is the route followed in [24]. Unfortunately, the resulting baryon asymmetry is too small to be simultaneously in accord with EDM constraints and the observed baryon asymmetry (a more extensive account of these results is given in Section 4.4).

The first study that does not rely on the assumption of fast oscillations was presented in [20, 23] for a toy model. In this regime, the interplay of off-diagonal and diagonal parts in the flavor space is more involved, which can lead to a parametric enhancement of *CP* violation in diagonal particle densities. In a bosonic toy model, the modes that are most affected by *CP* violation are the ones where the oscillation frequency is comparable to the background gradients, $\tau_\mathrm{osc} \sim l_\mathrm{w}$. In the MSSM, as argued above, these particles are rather hard, and this leads potentially to suppression, since these hard modes are not very abundant in the plasma. Still, it might turn out that these modes contribute to the *CP*-violating particle densities more than the bulk of particles in the adiabatic regime. Settling this issue would require an analysis along the lines of [20, 23] in a fermionic system (namely, the chargino sector of the MSSM), which is a daunting task.

[3] Nominally, they are of the second order in gradients and compatible with the semiclassical force terms.

2.6 Other approaches

In this section, we briefly discuss to what extent the approach presented in the last section is consistent with other methods found in the literature. In particular, we discuss the semiclassical force in the WKB approximation and the mass insertion formalism.

2.6.1 Semiclassical force in the WKB approximation. Historically, the semiclassical force was initially found in the WKB approximation [25–28] and subsequently applied to the MSSM [29–32]. The derivation is a little less clean than the one in the Kadanoff–Baym framework. For example, it relies on the quasiparticle picture, which is a stronger requirement than the mere gradient expansion used in the KB approach.

The derivation goes as follows: we again assume one fermionic particle species with a space–time-dependent complex mass term $m = |m| \exp(\mathrm{i}\theta)$. The corresponding Lagrangian is

$$\mathcal{L} = \bar{\psi}(\mathrm{i}\partial\!\!\!/ - P_{\mathrm{L}} m - P_{\mathrm{R}} m^*)\psi \,. \tag{53}$$

Using a local axial transformation, the Lagrangian can be brought to a form where the mass term is real, but an axial gauge field appears:

$$\mathcal{L} = \bar{\psi}(\mathrm{i}\partial\!\!\!/ + \gamma_5 Z\!\!\!/ - m)\psi \,, \tag{54}$$

where $Z_\mu = (1/2)\partial_\mu \theta$. Solving the Dirac equation then leads to the dispersion relation of quasiparticles. In the wall frame, we find [26, 27]

$$E^2 = p_\perp^2 + \left(\sqrt{p_z^2 + m^2} \pm Z_z\right)^2 . \tag{55}$$

The different signs denote the spin in the z-direction in the frame with vanishing $p_\perp$, similarly to the construction in the Kadanoff–Baym approach [see formula (44)]). The group velocity of the particle is given by

$$v_{\mathrm{g}} = \dot{z} = \frac{\partial E}{\partial p_z} \,, \tag{56}$$

and energy conservation gives the constraint

$$\dot{E} = 0 = \dot{z}\,\frac{\partial E}{\partial z} + \dot{p}_z\,\frac{\partial E}{\partial p_z} \,; \tag{57}$$

hence, $\dot{p}_z = -\partial_z E$. From these relations, the Boltzmann equation can be derived:

$$\frac{\mathrm{d}n}{\mathrm{d}t} = \partial_t n + \dot{z}\,\partial_z n + \dot{p}_z \partial_{p_z} n = \mathrm{coll.} \tag{58}$$

We note that the relation $\dot{p}_z = -\partial_z E$ ensures that for a static wall, the equilibrium particle distribution function (which in this case only depends on energy in the wall frame) is a solution of the Boltzmann equation.

We compare this result with our findings in the Kadanoff–Baym approach. In the $(1+1)$-dimensional case and for small gradients, we find

$$E^2 = \left(\sqrt{p_z^2 + m^2} \pm Z_z\right)^2 \simeq p_z^2 + m^2 \pm 2EZ_z \,. \tag{59}$$

Comparing this with (46), we see that the force in the WKB approximation is smaller by the factor m^2/E^2, which is close to unity for nonrelativistic particles. Therefore, the result is in rough agreement with the ones obtained later in the Kadanoff–Baym framework. However, the *CP*-violating term arises via an (axial) gauge transformation, which initially led to some discussion in the literature about whether this effect is physical. This issue can be resolved by distinguishing between canonical and physical momenta [31]. This careful analysis also recovers the factor m^2/E^2 and is then in full agreement with the result from the Kadanoff–Baym framework.

In conclusion, the derivation of the leading-order effect in the Kadanoff–Baym framework agrees with the one in the WKB approximation for one fermionic flavor. Nevertheless, the Kadanoff–Baym framework overcame some shortcomings of the semiclassical analysis. First, the above ambiguity involving the canonical and physical momenta never arises. Second, the Kadanoff–Baym framework does not assume quasiparticle states from the start. The quasiparticle properties are rather a consequence of the constraint equations in the lowest orders in the gradient expansion.

2.6.2 Mass insertion formalism. Another approach to *CP*-violating sources in transport equations is the mass insertion formalism [33–44]. Compared to the full-fledged Kadanoff–Baym treatment, the formalism has the advantage that it is perturbative, making even calculations with several flavors straightforward. The main application of this formalism is electroweak baryogenesis in the MSSM.

The main idea is to treat the mass term as an interaction and expand the Kadanoff–Baym equations around a plasma with vanishing mass. Formally, the fermionic equivalent of Eqn (23),

$$\left(p\!\!\!/ - P_{\mathrm{L}} m - P_{\mathrm{R}} m^\dagger - \Sigma(p, X)\right) \star\, S(p, X) = 1 \,, \tag{60}$$

is solved perturbatively (neglecting the terms Σ arising from 'real' interactions):

$$p\!\!\!/ \star\, S^{(1)} = (P_{\mathrm{L}} m + P_{\mathrm{R}} m^\dagger) \star\, S^{(0)} \,, \tag{61}$$

where S^0 denotes the equilibrium solution of a massless particle.

On general grounds, this formalism gives rise to several objections [45].

• In the case of one flavor, the main effect comes from a shift in the dispersion relation. This effect can be taken into account correctly only if the Kadanoff–Baym equations are solved. In the perturbative picture, the Kadanoff–Baym equations give rise to an infinite set of diagrams. Even worse, if the operator $p\!\!\!/ \star$ in (61) is inverted, we encounter divergences that have to be dealt with. As a simple example, we consider the following equation that mimics the constraint equation:

$$(x - a - \Delta a) f(x) = 0 \,, \tag{62}$$

with the solution $f(a) \propto \delta(x - a - \Delta a)$. If the equation is expanded in Δa, we find $f^{(0)}(a) \propto \delta(x - a)$ and $f^{(1)}(a) = \Delta a f^{(0)}/(x - a)$, which is not well defined. The correct behavior can in principle be recovered if we identify $\delta(x-a)/(x-a) \to -\delta'(x-a)$. But in the literature on electroweak baryogenesis, the problem is usually avoided by introducing a finite width in the spectral function. Potentially, this leads to an overestimation of the effect. Without expanding in Δa, the result is manifestly finite.

• By construction, the resulting Wightman function is local and does not therefore contain any transport. To

overcome this problem, the resulting deviation from equilibrium is interpreted as a source term and subsequently inserted into the transport equation to make diffusion possible. In the literature, different proposals exist regarding how this has to be done, the most plausible being the use of Fick's law [42].

• Flavor oscillations are not correctly reproduced in studies based on the mass insertion formalism.

• Once the source is inserted into the (classical) transport equations, a basis choice has to be made. The observation is that the *CP*-violating source vanishes in the mass eigenbasis, and the interaction eigenbasis is used. On the other hand, semiclassical quasiparticles propagate as mass eigenstates, making this choice questionable. The transport equations obtained in the Kadanoff–Baym framework are, in principle, basis independent.[4]

In Ref. [42], a refined version of the mass insertion formalism was presented. The mass was expanded around a fixed point:

$$m(X) = m(X^0) + (X_\mu - X^0_\mu)\,\partial_\mu m\,. \tag{63}$$

The derivative term was again treated as an interaction, while the mass term was incorporated into the lowest-order solution $S^{(0)}$. This overcame some of the problems listed above, but also reduced the predicted baryon asymmetry by one order of magnitude. In this partially resummed form, the main differences between the mass insertion formalism and the Kadanoff–Baym equations seem to be the implementation of transport and the neglect of flavor oscillations. While Boltzmann-type equations arise naturally in the Kadanoff–Baym equations, the mass insertion formalism still requires the use of Fick's law or some other classical input to describe transport.

A quantitative comparison between the different approaches in the MSSM is given in Section 4.4.

3. Electroweak baryogenesis: a toy model

In this section, we connect the analysis of *CP*-violating particle densities with an explicit calculation of the baryon asymmetry. Namely, we discuss how to pass from Boltzmann to diffusion equations (mostly in the cases without flavor mixing). Finally, we exemplify the complete calculation in a toy model. Some ingredients, such as the weak sphaleron rate and the characteristics of the phase transition, are covered in the appendices.

3.1 From Boltzmann to diffusion equations

Solving partial differential equations (48) or (50) is rather demanding without further approximations. In what follows, we discuss only the diffusion equations in models without flavor mixing, where the semiclassical force is the dominant source of *CP* violation.

We consider a Boltzmann-type equation in the wall frame of the form

$$p_z \partial_z n(\mathbf{p}) + mF_z\,\partial_{p_z} n(\mathbf{p}) = \text{coll.} \tag{64}$$

To simplify these partial differential equations further, the so-called flow ansatz is often used. The underlying assumption is that equilibration involves different time scales [46, 47]. When out of equilibrium, the system establishes kinetic equilibrium after a short time by decoherence effects and scattering processes. After this phase, the particle distribution functions of individual species are approximately of the form

$$n(\mathbf{p}) = \left.\frac{1}{\exp\left(u_\mu p^\mu + \mu\right)/T \pm 1}\right|_{p_0=\omega}, \tag{65}$$

where u^μ denotes the plasma four-velocity, T is the temperature, and μ is the chemical potential. At intermediate times, these quantities are still space–time dependent. Only at later times do the temperature and the four-velocity of the different species equilibrate to each other and the chemical potentials approach an equilibrium consistent with the conserved charges of the system. Similarly, in electroweak baryogenesis, the flow ansatz is fulfilled reasonably well everywhere, while the correct equilibrium is only attained away from the wall. Furthermore, it is usually also a good assumption in electroweak baryogenesis to use the same temperature for different species. This is owing to the special structure of the *CP*-violating source.[5]

Before we solve the Boltzmann equations using this ansatz, we discuss the connection to the Kadanoff–Baym equations in Section 2 in more detail. In the Kadanoff–Baym equations, the distribution functions for antiparticles are given by the negative-frequency part using the identification

$$\bar{n}(p^0) = -n(-p^0) \pm 1\,. \tag{66}$$

Hence, antiparticles come in flow ansatz (65) with the same four-velocity and temperature but opposite chemical potential, as it should be. Of course, in the presence of *CP* violation, small deviations between the chemical potentials and velocities of particles and antiparticles can arise. Another important point is how to relate the *CP*-violating force to the system of Boltzmann equations. The Boltzmann equations do not contain the full Dirac structure of the Kadanoff–Baym approach but only parameterize the system by four densities of (pseudo) particles. Typically, these are chosen to be left-/right-chiral particles/antiparticles. By contrast, in the Kadanoff–Baym approach, spin is a conserved quantum number. To translate semiclassical force (48) into the chirality basis, the force is transformed into

$$mF_z \simeq \frac{1}{2}\,|m^2|' \pm \frac{\operatorname{sign} p_z}{2\omega}\,\left(|m^2|\theta'\right)', \tag{67}$$

where opposite signs respectively apply for left/right-chiral densities and particles/antiparticles. Strictly speaking, this identification is only true for highly relativistic particles, but we see below that it reproduces (in the leading order in wall velocity) the correct deviation from equilibrium in terms of vector and axial currents.

Using the flow ansatz, different moments of transport equation (64) can then be taken in order to reduce the Boltzmann-type equation to a diffusion-type equation. This leads to the relations

$$\begin{aligned} &\langle p_z\rangle\mu' + \langle p_z^2\rangle u_z' + \langle mF_z\rangle u_z = \langle\text{coll.}\rangle\,,\\ &\langle p_z^2\rangle\mu' + \langle p_z^3\rangle u_z' + \langle p_z mF_z\rangle u_z = \langle p_z\,\text{coll.}\rangle\,, \end{aligned} \tag{68}$$

[4] However, in practice, a basis choice is also often made in the Kadanoff–Baym framework when the particle densities are coupled to other species (see, e.g., [24]). Therefore, the problem is in fact only postponed.

[5] In the calculation of the wall velocity, this would be a poor approximation [48].

where u_z is in the leading order given by the flow of the background (that equals the wall velocity far away from the wall). We used the fact that the flow term and the force satisfy the relations $\mathrm{d}\omega/\mathrm{d}p_z = p_z/\omega$ and $\mathrm{d}\omega/\mathrm{d}z = m F_z/\omega$, which ensures that the two derivative terms acting on the energy ω cancel each other.[6]

The moments are usually defined as

$$\langle X\rangle = \frac{1}{N}\int \mathrm{d}^3p\ \frac{1}{\omega}\frac{\mathrm{d}n}{\mathrm{d}\mu}\,X\,, \tag{69}$$

with the normalization to a fermionic massless degree of freedom in equilibrium:

$$N = \int \mathrm{d}^3p\ \frac{\mathrm{d}n_\mathrm{f}}{\mathrm{d}\mu}\bigg|_{m=\mu=u_z=0}\,. \tag{70}$$

In what follows, we linearize the system in the chemical potentials and the flow velocities. In the leading order, certain moments are then related by Lorentz boosts, e.g., $\langle p_z\rangle \simeq -u_z\kappa$, where $\kappa \equiv \langle\omega\rangle$ denotes the statistical factor that is 1 (2) for massless fermions (bosons) for a plasma at rest. Furthermore, $\langle p_z^2\rangle$ is in the leading order 1/3 of the pressure in the plasma and $\langle p_z^3\rangle \simeq -3u_z\langle p_z^2\omega\rangle$.

Next, we consider the collision terms. The collision integral in the second equation is dominated by elastic scatterings:

$$\langle p_z\,\mathrm{coll.}\rangle \simeq -\Gamma^\mathrm{ela}(u-\bar u) \tag{71}$$

(note that Γ^ela has dimension three according to this definition). The function $\bar u$ denotes the flow velocity of the background with which the species mostly scatters, and it is often assumed that this is given by the wall velocity that describes the flow far away from the wall, $\bar u \simeq v_\mathrm{w}$. We note that this approximation is in general consistent with the arguments of energy–momentum conservation discussed in Section 2.3. Still, as long as the background represents a large number of degrees of freedom, this approximation is reasonable.

The collision term in the first equation encodes the particle-changing interactions. These have the form

$$\langle\mathrm{coll.}\rangle \simeq \Gamma^\mathrm{inela}\sum_i c_i\,\mu_i\,, \tag{72}$$

where c_i are some integer constants and the subscript i labels the species of the chemical potentials μ_i. One of these interactions constitutes the sphaleron rate that eventually leads to the formation of baryon asymmetry. Both sphaleron rates, strong and electroweak, are nonperturbative, and neither can be recovered from the collision term as given in (25). They have to be added by hand to the network of transport equations.

Finally, we consider the forces in the diffusion equation. The *CP*-conserving force drives the flow of particles and antiparticles equally away from equilibrium,

$$\langle mF_z\rangle u_z \simeq \frac{1}{2}\,|m^2|'\langle 1\rangle v_\mathrm{w} \equiv S_\mu\,, \tag{73}$$

but does not have a large impact on chemical potentials. The *CP*-violating force, on the other hand, contributes mostly to the equation involving the chemical potential:

$$\langle p_z m F_z\rangle u_z \simeq \frac{1}{2}\left(|m^2|\theta'\right)'\left\langle\frac{|p_z|}{\omega}\right\rangle v_\mathrm{w} \equiv S_u\,. \tag{74}$$

In particular, the *CP*-violating force comes with different signs for the left- and right-chiral fields, and it therefore has an impact only on the axial current, as found in the Kadanoff–Baym approach. Moreover, it explicitly vanishes for static walls.

This system of equations can be brought to the form of a diffusion equation by neglecting terms that are of the second order in the velocities in the second equation. This gives

$$u-\bar u \simeq \frac{1}{\Gamma^\mathrm{ela}}\left(\langle p_z^2\rangle\,\mu' + S_u\right). \tag{75}$$

Neglecting derivatives acting on the averages and using this in (68) yields

$$D\mu'' + v_\mathrm{w}\kappa\mu' + S_\mu + S_D = \langle\mathrm{coll.}\rangle\,, \tag{76}$$

where we define the diffusion constant

$$D = \frac{\langle p_z^2\rangle^2}{\Gamma^\mathrm{ela}}\,, \tag{77}$$

and the *CP*-violating source of the form $S_D = S_u'/\Gamma^\mathrm{ela}$. However, there is no need for these additional approximations, and linear differential equations (68) can be easily solved numerically.

In conclusion, after linearization in the velocities and the chemical potentials, the system of transport equations can be brought to the form

$$\partial_z\Delta J_\alpha^z + \sum_{A,\beta}\Gamma_A^\mathrm{inela}c_\alpha^A c_\beta^A\mu_\beta = 0\,, \tag{78}$$

$$\partial_z\Delta T_\alpha^{zz} + \Gamma_\alpha^\mathrm{ela}(u_\alpha - v_\mathrm{w}) = S_\alpha\,, \tag{79}$$

where the indices α and β range all particle species and chiralities and the index A ranges all interactions. The term ΔJ^z denotes the current of particles minus antiparticles, and the expression $\partial_z\Delta J^z$ represents all three terms in the left-hand side of the first equation in (68). Likewise, the term ΔT^{zz} denotes the zz component of the energy–momentum tensor of particles minus antiparticles, and the expression $\partial_z\Delta T_\alpha^{zz}$ represents the first two terms of the second equation in (68). On the other hand, the *CP*-violating contribution of the force is treated as a source, S_α. $\Gamma_\alpha^\mathrm{ela}$ represents elastic scattering rates while Γ_A^inela stands for the interaction rates that change the particle number and involve the chemical potentials μ_β. The vectors c_α^A specify which particles participate in a specific interaction.

A conserved current can be represented by a vector d_α. In this case, all interactions have to preserve the current, $\sum_\alpha c_\alpha d_\alpha = 0$, and the current should have no source, $\sum_\alpha d_\alpha S_\alpha = 0$. An example of conserved quantities are the electric charge in the broken phase or the baryon number if the weak sphaleron process is neglected.

3.2 Simple diffusion network

To determine the final baryon asymmetry, we have to set up a set of transport equations that contains all relevant degrees of

[6] Generally, an additional term arises from derivatives acting on the term sign p_z, but these turn out to be negligible [49].

freedom. The sphaleron rate is one of the smallest interaction rates in this system, and it therefore suffices to neglect back reactions and determine the net baryon number from the left-handed particle density, as is described at the beginning of Appendix A.

In our toy model, the *CP*-violating source is in the top sector, and we first consider all fast interaction rates involving top quarks. These are the Yukawa interactions with the Higgs boson, the electroweak interactions with W bosons, and the strong sphaleron rate that involves all quarks. In the broken phase, the Higgs vev induces chiral flips between left- and right-handed tops, and the Higgs bosons decay into W bosons. The relevant particle-changing interaction rates are [34, 50]

$$\begin{gathered} \mathrm{t_L} \leftrightarrow \mathrm{t_R} + \mathrm{h} : \Gamma_\mathrm{y} \simeq 4.2 \times 10^{-3} T, \\ \mathrm{t_L} \leftrightarrow \mathrm{t_R} : \Gamma_\mathrm{m} \simeq \frac{m_\mathrm{t}^2}{63T}, \\ \mathrm{t_L} + \mathrm{b_L} + 4\mathrm{u_L} \leftrightarrow \mathrm{t_R} + \mathrm{b_R} + 4\mathrm{u_R} : \Gamma_\mathrm{ss} \simeq 4.9 \times 10^{-4} T, \\ \mathrm{h} \leftrightarrow 2\mathrm{W} : \Gamma_\mathrm{h} \simeq \frac{m_\mathrm{W}^2}{50T}, \end{gathered} \tag{80}$$

where $\mathrm{u_L}$ and $\mathrm{u_R}$ collectively denote the left- and right-handed light quarks.

Next, the elastic scattering rates of the Higgs boson and the top quark have to be specified. These are usually given in terms of the diffusion constants defined in (77) and calculated in [26, 27, 31, 51–53]:

$$D_\mathrm{q} \equiv \frac{6}{T}, \quad D_\mathrm{h} \equiv \frac{20}{T}. \tag{81}$$

The Higgs and W bosons decay quickly in the broken phase, and hence neglecting their chemical potential does not have a large impact on the final baryon asymmetry. A detailed analysis concerning this point can be found in [49]. Furthermore, the interactions with the W bosons are rather fast, and hence left-handed up and down quarks have similar chemical potentials. The right-handed bottom quark and the light quarks are only sourced by the strong sphaleron rate and otherwise interact only with very small Yukawa interactions. Hence, the chemical potential of the light right-handed quarks equals that of the right-handed bottom quark, while the light left-handed quarks have the opposite chemical potential.

Up to this point, the remaining degrees of freedom are the left-handed top and bottom quarks with the chemical potential μ_q, and the right-handed top and bottom quarks with the respective chemical potentials μ_t and μ_b. The light right-handed quarks have the same chemical potential as the right-handed bottom quark, μ_b, and the light left-handed quarks have the opposite chemical potentials.

The baryon number conservation then relates these chemical potentials as

$$(\kappa_\mathrm{t} + 1)\mu_\mathrm{q} + \mu_\mathrm{b} + \kappa_\mathrm{t}\mu_\mathrm{t} = 0. \tag{82}$$

The light quarks cancel in this equation, since left- and right-handed particles have opposite chemical potentials. We also neglect the bottom masses, $\kappa_\mathrm{b} = \kappa_0 = 1$. The chemical potential of the right-handed bottom quark can then be eliminated in the remaining network. For example, the strong sphaleron couples to the combination

$$2\mu_\mathrm{q} - \mu_\mathrm{t} - 9\mu_\mathrm{b} = (9\kappa_\mathrm{t} + 11)\mu_\mathrm{q} + (9\kappa_\mathrm{t} - 1)\mu_\mathrm{t}. \tag{83}$$

Here, the term $-9\mu_\mathrm{b}$ represents the nine light quark chiralities, including the right-handed bottom quark. Ultimately, the left-handed baryon chemical potential entering the sphaleron process [see Eqn (122) in Appendix A] is given by

$$\mu_\mathrm{L} = \mu_\mathrm{q} - 2\mu_\mathrm{b} = (3 + 2\kappa_\mathrm{t})\mu_\mathrm{q} + 2\kappa_\mathrm{t}\mu_\mathrm{t}. \tag{84}$$

The contribution $-2\mu_\mathrm{b}$ represents the left-handed quarks of the two light families. We note that if the top quark is assumed to be light, $\kappa_\mathrm{t} = 1$, then the combination of the chemical potentials that enters the weak sphaleron process, Eqn (83), is proportional to the combination of chemical potentials that enters the strong sphaleron process, Eqn (84). Hence, in this limit, the final baryon asymmetry is suppressed by the strong sphaleron rate [54].

We do not quote the full set of equations here. The explicit equations for a network including the Higgs and W-boson fields can be found, for example, in Ref. [49]. A reduced network without a Higgs field has been used in Refs [55, 56]. A generalization to the two-Higgs-doublet model is given in Ref. [57]. Also, the generalization to supersymmetric extensions is extensively discussed in the literature. This includes new damping rates [58] but also much more complicated diffusion networks. In many cases, it is assumed that supergauge interactions are in equilibrium, such that particle species and their superpartners share the same chemical potential. If this assumption is relaxed, the outcome of the diffusion network depends on many more parameters, such as the mass spectrum of all the superpartners. This can lead to very large correction and even to a change of sign in the final baryon asymmetry [59–61].

In what follows, we present some results from [56]. To provide as model-independent results as possible, the source in the top sector is parameterized via the mass term as

$$m_\mathrm{t} = y_\mathrm{t}\,\phi(z)\exp\left(\mathrm{i}\Theta_\mathrm{t}(z)\right),$$

using

$$\begin{aligned} \phi(z) &= \frac{\phi_\mathrm{c}}{2}\left(1 + \tanh\frac{z}{l_\mathrm{w}}\right), \\ \Theta_\mathrm{t}(z) &= \frac{\Delta\Theta_\mathrm{t}}{2}\left(1 + \tanh\frac{z}{l_\mathrm{w}}\right). \end{aligned} \tag{85}$$

The final asymmetry is then proportional to the change in the top-quark mass phase during the phase transition, $\Delta\Theta_\mathrm{t}$. Otherwise, it only depends on the dimensionless quantities $\phi_\mathrm{c}/T_\mathrm{c}$ and $l_\mathrm{w}T_\mathrm{c}$.

Figure 3 shows the change $\Delta\Theta_\mathrm{t}$ in the top-quark mass phase during the phase transition required in order to reproduce the observed baryon asymmetry. The baryon asymmetry is very sensitive to the strength of the phase transition, $\phi_\mathrm{c}/T_\mathrm{c}$. Furthermore, as expected, a larger wall thickness reduces the produced asymmetry. For phase transitions that barely satisfy the baryon wash-out criterion $\phi_\mathrm{c} \simeq T_\mathrm{c}$, a change of phase $\Delta\Theta_\mathrm{t} \gtrsim 0.3 - 0.6$ is required for realistic wall thicknesses $l_\mathrm{w}T_\mathrm{c} \simeq 2-8$.

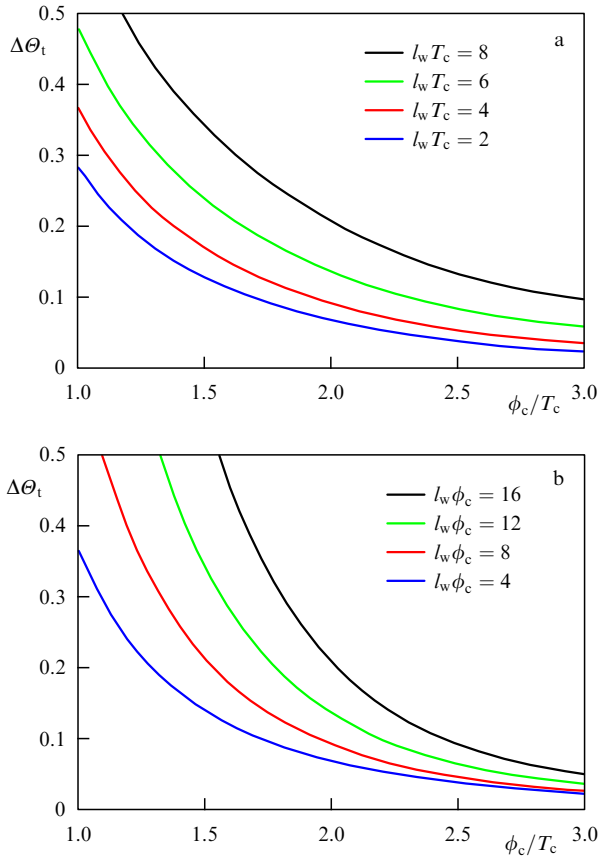

Figure 3. The change $\Delta\Theta_t$ in the top-quark mass phase during the phase transition needed to reproduce the observed baryon asymmetry. In the upper plot, the wall thickness in terms of the temperature is kept constant, while in the bottom plot, the wall thickness in terms of the critical vev is kept constant. The plots are adapted from Ref. [56].

4. Models

The crucial ingredients of electroweak baryogenesis are a strongly first-order phase transition and an appropriate source of *CP* violation.

A strong electroweak phase transition is needed for several reasons. First, the nucleated bubbles during the first-order phase transition are the source that drives the plasma locally out of equilibrium and facilitates the establishment of sizable *CP*-violating currents. Second, the baryon-number-violating sphaleron processes have to be sufficiently suppressed after the phase transition in order to avoid the wash-out of the baryon asymmetry just produced. This leads to a constraint on the Higgs vev ϕ_c and the phase transition temperature T_c of the form

$$\frac{\phi_c}{T_c} > 1.1 \tag{86}$$

(see Appendix A for a short derivation of this bound). It is well known that in the SM, a first-order phase transition is excluded for Higgs masses beyond roughly the W-boson mass [62]. To fulfill wash-out criterion (86), a Higgs mass below ~ 40 GeV would even be necessary. This is in contrast to the Higgs mass bound $m_H > 114$ GeV from LEP. Generally, a strong phase transition satisfying (86) requires either an extended scalar sector or at least new degrees of freedom that are strongly coupled to the Higgs boson.

In electroweak baryogenesis, an appropriate source of *CP* violation has to be in the form of a complex mass matrix that changes during the phase transition, such that a chiral flux is generated close to the bubble wall. This is achieved by coupling the corresponding particles to a vev that constitutes the nucleating bubbles of the phase transition. In many cases, this vev arises from the physical Higgs field, but more complicated scalar sectors tend to increase the prospects of electroweak baryogenesis, because the masses of the SM fermions are proportional to the Higgs vev. A comparison with the sources in (48) then shows that *CP* violation is absent. Hence, either the masses of the SM fermions need to be modified, or a new fermionic particle is responsible for the *CP*-violating flux. In the latter case, the *CP*-violating flux has to ultimately influence the sphaleron rate. Hence, this new degree of freedom is in many models charged under $SU(2)_L$.

At the same time, these new features can leave traces in collider and low-energy probes. One major constraint comes from electric dipole moments that constrain new sources of *CP* violation. Often, the induced electric dipole moments arise only in the second loop. Still, current bounds on the electron EDM, $d_e < 1.05 \times 10^{-27}\, e\,\text{cm}$ [63], and neutron EDM, $d_n < 2.9 \times 10^{-26}\, e\,\text{cm}$ [64], heavily constrain realistic models of electroweak baryogenesis. Also, the new degrees of freedom responsible for a strong phase transition can have measurable implications. The prime example of this is the MSSM, where only light right-handed stops can yield a sufficiently strong phase transition. Such light stops would be copiously produced at the LHC, which leads to additional constraints.

In what follows, we discuss several models in which electroweak baryogenesis is feasible. We start with relatively simple models with higher-dimension operators and the two-Higgs-doublet model in which the semiclassical force is operative. Then we discuss the MSSM and its extensions, which requires a more sophisticated treatment of *CP* violation from flavor mixing.

4.1 Standard Model with a low cutoff

From the bottom-up perspective, the minimal approach to extensions of the SM is to insist on the particle content of the SM and only extend the Lagrangian by higher-dimension operators. Since electroweak baryogenesis requires sizable deviations from the SM at around the weak scale, the suppression of higher-dimension operators and the physical cutoff of the theory cannot be much larger in this framework. Still, the higher-dimension operators can have an important impact on the phase transition, provide new sources of *CP* violation, and make electroweak baryogenesis a viable option.

4.1.1 Phase transition. The leading operator that modifies the Higgs potential has the form $(\Phi^\dagger\Phi)^3$, and the scalar potential of the Higgs vev ϕ is then given by

$$V(\phi) = \mu^2\phi^2 + \lambda\phi^4 + \frac{1}{\Lambda^2}\,\phi^6\,. \tag{87}$$

The new scale Λ is the cutoff of the theory, where new degrees of freedom become relevant, or at least strong-coupling phenomena occur. This form of the potential can lead to a strong phase transition already in the mean-field approximation, where temperature effects only contribute to the quadratic Higgs term, $\Delta V_T \simeq c\,T^2\phi^2$. The barrier is then

produced by balancing a negative quartic term, $\lambda < 0$, with the positive ϕ^6 operator [65, 66]. The critical temperature is then

$$T_c^2 = \frac{\Lambda^4 m_H^4 + 2\Lambda^2 m_H^2 \phi_0^4 - 3\phi_0^8}{16 c \Lambda^2 \phi_0^4}\,, \tag{88}$$

where the parameters μ and λ are expressed in terms of the physical Higgs mass m_H and the observed Higgs vev $\phi_0 \simeq 246$ GeV. The critical vev is given by

$$\phi_c^2 = \frac{3}{2}\,\phi_0^2 - \frac{m_H^2 \Lambda^2}{2\phi_0^2}\,. \tag{89}$$

There is also an upper limit on Λ where the phase transition becomes a second-order one and a lower bound from the fact that the broken phase is the global minimum at $T = 0$. As usual, an increase in the Higgs mass makes the phase transition weaker. Wash-out criterion (86) translates into an upper bound on Λ. In the full one-loop analysis, the values are [66]

$$\begin{aligned} &\Lambda \lesssim 800\ \text{GeV}\,, \qquad m_H = 125\ \text{GeV}\,,\\ &\Lambda \lesssim 900\ \text{GeV}\,, \qquad m_H = 115\ \text{GeV}\,. \end{aligned} \tag{90}$$

A peculiar feature of the model seems to be that the coefficient of the quartic λ is negative. However, a negative quartic can arise quite naturally in effective actions, for example, when a heavy scalar is integrated out [65].

4.1.2 Electroweak baryogenesis. Electroweak baryogenesis was considered for this model in [55]. As an additional efficient source of *CP* violation, a dimension-six coupling between the Higgs field Φ and the up quarks,

$$\mathcal{L} \ni \frac{x_{ij}}{\Lambda_{CP}^2}(\Phi^\dagger \Phi)\bar{q}_i \Phi u_j + \text{h.c.}, \tag{91}$$

was used in combination with the usual Yukawa coupling,

$$\mathcal{L} \ni y_{ij}\,\bar{q}_i \Phi u_j + \text{h.c.} \tag{92}$$

The resulting fermion masses during the phase transition are given by

$$m_{ij} = y_{ij}\,\frac{\phi}{\sqrt{2}} + x_{ij}\,\frac{\phi^3}{\sqrt{8}\,\Lambda_{CP}^2}\,, \tag{93}$$

which leads to a *CP*-violating semiclassical force if there are relative complex phases between y_{ij} and x_{ij}. The most important effect is in the top sector, since the other quarks are too light to yield a sizable *CP*-violating flux along the bubble wall. The change in the phase is hence

$$\Delta\theta \simeq \text{Im}\,(x_t)\,\frac{\phi^2}{\Lambda_{CP}^2}\,, \tag{94}$$

where x_t denotes the 33 element of the x_{ij} coupling in the mass eigenbasis of the quarks.

The system of transport equations is the one discussed in Section 3.2. The only degrees of freedom are those from the Standard Model, and the dominant source of *CP* violation is the semiclassical force in the top sector. The only missing ingredient in the present context is the wall thickness. A numerical analysis of all the characteristics of the phase transition (Fig. 4) and the analysis of the produced baryon asymmetry is given in Ref. [55]. The final baryon asymmetry is very sensitive to the scale Λ. The main influence comes from the relation between Λ and the critical Higgs vev ϕ_c. Semiclassical force (67) is proportional to ϕ_c^2 via the top-quark mass and another factor ϕ_c^2 comes from the change in the phase (94). In addition, the wall thickness l_w tends to be smaller for stronger phase transitions, and hence lower values of Λ. The calculated baryon asymmetry is consistent with the observed values $\text{Im}\,(x_t) \lesssim 1$ and the bound $\Lambda_{CP} \simeq \Lambda < 650$ GeV.

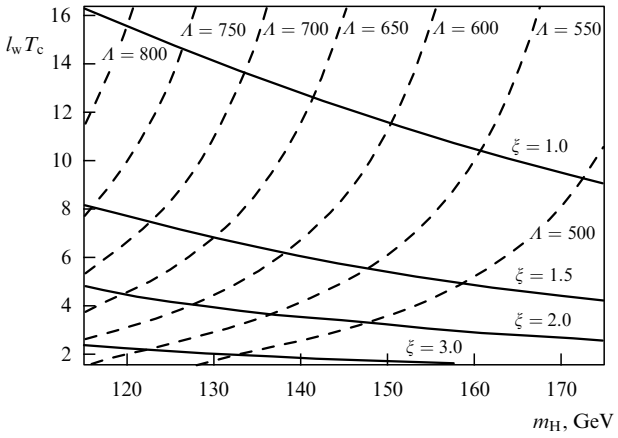

Figure 4. The wall thickness l_w as a function of the Higgs mass. The plot also shows the corresponding values of the new physics scale Λ and the ratio $\xi = \phi_c/T_c$. Plot adapted from [55].

4.1.3 Collider and low-energy probes of the model. Since the model does not contain any new degrees of freedom, no spectacular signatures are expected in colliders. Still, higher-dimension operators can lead to measurable deviations from the SM.

In connection with the phase transition, the new operator ϕ^6 is an essential ingredient. The main collider trace of this new operator is a deviation of the self-couplings of the Higgs field in terms of the Higgs mass [65]. The deviations from the SM couplings are

$$\mu = 3\,\frac{m_H^2}{\phi_0} + 6\,\frac{\phi_0^3}{\Lambda^2}\,, \qquad \eta = 3\,\frac{m_H^2}{\phi_0^2} + 36\,\frac{\phi_0^2}{\Lambda^2}\,, \tag{95}$$

where μ (η) denotes the cubic (quartic) self-coupling of the Higgs field. The deviations are pronounced for small Higgs masses, e.g., $\mu \simeq 2\mu_{SM}$ for $m_H = 125$ GeV and $\Lambda = 650$ GeV. Still, the discovery of a deviation of this size requires a linear collider [65]. However, in combination with EDM bounds, viable baryogenesis requires an even stronger phase transition that makes even larger deviations in the Higgs sector necessary. This is discussed next.

The new source of *CP* violation gives potentially much stronger bounds in light of the observed limits on flavor-changing neutral currents. However, these bounds are more model dependent and notably hinge on the flavor structure x_{ij} of the new operator (91). Flavor-changing neutral currents potentially arise, because mass term (93) is not proportional to the coupling between the Higgs field and the fermions:

$$Y_{ij} = y_{ij}\,\frac{1}{\sqrt{2}} + x_{ij}\,\frac{3v^2}{\sqrt{8}\,\Lambda_{CP}^2}\,. \tag{96}$$

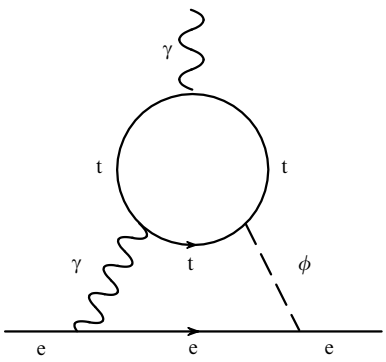

Figure 5. Two-loop contribution to the Barr–Zee electron EDM.

If the x_{ij} couplings were random numbers of the order of unity, large deviations in the first two quark families could be observed. For example, operator (91) would affect the $\mathrm{K}-\bar{\mathrm{K}}$ mixing [55], which implies a bound $\Lambda_{CP} \gtrsim 10^7$ GeV. If, on the other hand, x_{ij} has a flavor structure similar to y_{ij}, the model is consistent with these constraints as long as $\Lambda_{CP} > 500$ GeV. Such a setting agrees well with the hypothesis of minimal flavor violation [67] and can be achieved in Froggatt–Nielsen classes of models.

Constraints from the electric dipole moments are more robust, since they occur even in a one-flavor scheme with a relative phase between the couplings y_t and x_t. Because this phase is also essential for the formation of baryon asymmetry, this provides a direct link between low-energy observables and baryogenesis. The dominant constraints [68] come from the Barr–Zee contributions to the neutron and electron EDMs (Fig. 5). For the Higgs mass $m_\mathrm{H} = 125$ GeV, this constraint is $\Lambda_{CP} \gtrsim \sqrt{\mathrm{Im}\,(x_\mathrm{t})} \times 750$ GeV, and it becomes slightly weaker for larger Higgs masses.

4.1.4 Summary. Electroweak baryogenesis is a viable possibility in the Standard Model with a low cutoff. The strongest constraints on the model come from the cubic Higgs self-coupling and the upper bounds on the neutron EDM. On general grounds, we expect that the new operator in (87) that makes the phase transition strong and operators (91) that provide *CP* violation are of a similar size, $\Lambda \sim \Lambda_{CP}$. This is indeed possible for Λ somewhat smaller than Λ_{CP}. A possible set of parameters is, for example,

$$\Lambda \simeq 500\ \mathrm{GeV}, \quad \Lambda_{CP} \simeq 1000\ \mathrm{GeV}, \quad \mathrm{Im}\,(x_\mathrm{t}) \simeq 1\,. \tag{97}$$

If the Higgs boson is rather light ($m_\mathrm{H} \simeq 125$ GeV), this particular set of parameters will be tested in the near future. The cubic coupling is enhanced by a factor of ~ 3 compared to the SM, which could even be in reach of the high-luminosity LHC. Furthermore, the next generation of neutron EDM measurements (assuming an improvement in sensitivity by a factor of 10) can rule out this model of electroweak baryogenesis.

4.2 Low cutoff: singlet extension

The best motivation for extensions of the SM with a low cutoff comes from composite Higgs models, in which the light spectrum of the scalar sector depends on the co-set structure of the strongly coupled sector. The degrees of freedom below the scale of strong coupling arise as bound states with a pseudo-Goldstone nature. In the minimal model [69–71], the Higgs boson is a pseudo-Goldstone boson of the breaking pattern $\mathrm{SO}(5) \to \mathrm{SO}(4)$, where SO(4) represents the custodial symmetry of the Higgs sector. In nonminimal models, an extended scalar sector appears at low temperatures. In what follows, we discuss the model with the breaking pattern $\mathrm{SO}(6) \to \mathrm{SO}(5)$ that serves as a UV completion of the singlet extension of the SM with a low cutoff [72].

From a phenomenological standpoint, electroweak baryogenesis can be more easily realized in this model than in the SM with a low cutoff. First, the phase transition can already be strong with a renormalizable scalar potential and in the mean-field approximation and does not rely on higher-dimension operators at all. Second, the leading source of *CP* violation already arises at dimension five. This allows pushing the cutoff to a few TeV, which is advantageous in view of flavor physics. Last, the dominant contribution to the EDM constraints comes from a mixing between the Higgs field and the additional singlet degree of freedom. As long as this mixing is small, current constraints from low-energy probes are easily satisfied.

4.2.1 Phase transition. As mentioned above, the phase transition can already be strong in the mean-field approximation with only renormalizable operators in the scalar potential. Interestingly, this is even true if a $\mathbf{Z}_2$ symmetry is imposed on the singlet, $s \to -s$. We consider the following potential at the critical temperature:

$$V\Big|_{T=T_\mathrm{c}} = \frac{\lambda}{4}\left(\phi^2 + \frac{s^2\phi_\mathrm{c}^2}{s_\mathrm{c}^2} - \phi_\mathrm{c}^2\right)^2 + \frac{\kappa}{4}\,\phi^2 s^2\,. \tag{98}$$

The variables ϕ and s denote the Higgs and singlet vevs and ϕ_c and s_c the corresponding values of the vevs in the $\mathrm{SU}(2)_\mathrm{L}$ and $\mathbf{Z}_2$-breaking phases at the critical temperature. The first term constitutes a Mexican-hat potential with a flat direction that connects the $\mathrm{SU}(2)_\mathrm{L}$-breaking with the $\mathbf{Z}_2$-breaking phase. The second term lifts this flat direction and creates a barrier between the two degenerate minima of the potential.

Thermal corrections in the mean-field approximation can be added to this potential via

$$\Delta V_T = \frac{1}{2}(c_\phi\,\phi^2 + c_\mathrm{s} s^2)(T^2 - T_\mathrm{c}^2)\,, \tag{99}$$

where the two coefficients c_ϕ and c_s are [73]

$$\begin{aligned} c_\phi &= \frac{1}{48}\left(9g^2 + 3g'^2 + 12y_\mathrm{t}^2 + 24\lambda + 4\sqrt{\lambda\lambda_\mathrm{s}} + 2\kappa\right), \\ c_s &= \frac{1}{12}\left(3\lambda_\mathrm{s} + 4\sqrt{\lambda\lambda_\mathrm{s}} + 2\kappa\right) \end{aligned} \tag{100}$$

and we define $\lambda_\mathrm{s} = \lambda\phi_\mathrm{c}^4/s_\mathrm{c}^4$. In total, the model has four free parameters that can be fixed using the observed Higgs vev $\phi = 246$ GeV, the Higgs mass, the singlet mass, and the critical temperature. A lower bound on the singlet mass results from the requirement of a first-order phase transition ($\kappa > 0$), while an upper bound on the singlet mass arises from the requirement that the $\mathrm{SU}(2)_\mathrm{L}$-broken phase be the global minimum at $T = 0$. Detailed plots are given in [73] (also see [74]). For fixed Higgs and singlet masses, the critical temperature can always be reduced to the point where the system becomes very strong: $\phi_\mathrm{c}/T_\mathrm{c} \sim$ a few units.

In fact, the phase transition proceeds in two stages in this model: at very high temperatures, the singlet vev, as well as the Higgs vev, vanishes and neither the electroweak $\mathrm{SU}(2)_\mathrm{L}$

nor the $\mathbf{Z}_2$ symmetry is broken. At lower temperatures, the singlet develops a vev that breaks the $\mathbf{Z}_2$ symmetry. Depending on the parameters, this process can occur at several hundred GeV and is probably rather a crossover than a phase transition. At this stage, domain walls are generated. However, the domain walls are harmless to big bang nucleosynthesis, because they disappear in the next stage when the system transits from the $\mathbf{Z}_2$-breaking phase to the electroweak breaking one.

4.2.2 Electroweak baryogenesis. In contrast to the Standard Model with a low cutoff, its singlet extension already has a powerful source of *CP* violation at dimension five:

$$\mathcal{L} \ni \frac{x_{ij}}{\Lambda_{CP}}\, s\bar{q}_i \Phi u_j + \text{h.c.} \tag{101}$$

The resulting fermion masses during the phase transition are

$$m_{ij} = y_{ij}\,\frac{\phi}{\sqrt{2}} + x_{ij}\,\frac{s\phi}{\sqrt{2}\,\Lambda_{CP}}\,, \tag{102}$$

which again leads to a *CP*-violating semiclassical force if there are relative complex phases between y_{ij} and x_{ij}. Following the rationale of the SM with low cutoff, we focus on the top-quark sector. The change in the phase of the top-quark mass is of the order

$$\Delta\Theta_{\rm t} \simeq \text{Im}\,(x_{\rm t})\,\frac{s}{\Lambda_{CP}}\,, \tag{103}$$

where $x_{\rm t}$ again denotes the coupling in the mass eigenbasis of the quarks. The singlet extension has several advantages over the minimal model with cutoff from the standpoint of baryogenesis. First, the phase transition can be rather strong without coming into conflict with a low cutoff. Next, the change in phase (103) is only suppressed by one power of Λ, making baryogenesis in this model possible with a cutoff $\Lambda \sim 2-3$ TeV. With such a high cutoff, it is possible to solve the flavor problem using the 5D Glashow–Iliopoulos–Maiani (GIM) mechanism in specific realizations of the composite Higgs mechanism [75]. Furthermore, the singlet vev is expected[7] to be larger than the Higgs one, which further increases the source in (103). Some numerical results are shown in Fig. 6. Electroweak baryogenesis can be viable for $\Delta\Theta_{\rm t} \gtrsim 1$, translating into the bound $\Lambda_{CP} <$ a few TeV.

We note that if the scalar potential is completely $\mathbf{Z}_2$ symmetric, the baryon asymmetry is suppressed. As mentioned above, domain walls are generated at intermediate scales where the singlet vev breaks the $\mathbf{Z}_2$ symmetry spontaneously. At this stage, the Universe is divided into regions with positive/negative singlet vevs. These regions produce opposite baryon numbers during the electroweak phase transition. To avoid this problem, the $\mathbf{Z}_2$ symmetry has to be slightly broken. Even a very small breaking leads to the disappearance of domain walls and preserves the baryon asymmetry [56].

4.2.3 Collider and low-energy probes of the model. Unlike the SM case, the additional *CP*-violating operator does not give rise to dangerous flavor observables. First, if the model is approximately $\mathbf{Z}_2$-symmetric, operator (101) is absent after the electroweak phase transition. Even if the scalar field has a (small) vev after the electroweak phase transition, the Yukawa interactions with the fermions can be diagonalized simultaneously with fermionic mass terms (102), which suppresses flavor-changing neutral currents to a higher-loop order.

In terms of collider traces and electric dipole moments, deviations from the SM arise mostly from a singlet-Higgs mixing. As mentioned above, a very small $\mathbf{Z}_2$ breaking is required for viable baryogenesis, but it is easily compatible with bounds from electroweak precision tests or EDMs, as seen in Fig. 7.

Another characteristic signal of the model would be a Higgs boson decay into four fermions via two singlets. Whether this process can be tested depends, however, on the

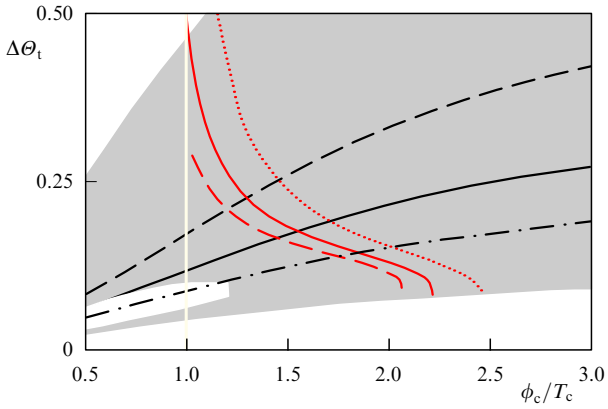

Figure 6. (Color online.) The shaded region shows possible models in the plane $\xi = \phi_{\rm c}/T_{\rm c}$ versus the change in the top-quark phase $\Delta\Theta_{\rm t}$. The Higgs and singlet masses are $m_{\rm H} = 120$ GeV and $m_{\rm s} = 130$ GeV. The scale of the new physics is $\Lambda_{CP} = 500$ GeV. The red lines denote the parameters that reproduce the observed baryon asymmetry. Plot adapted from [56].

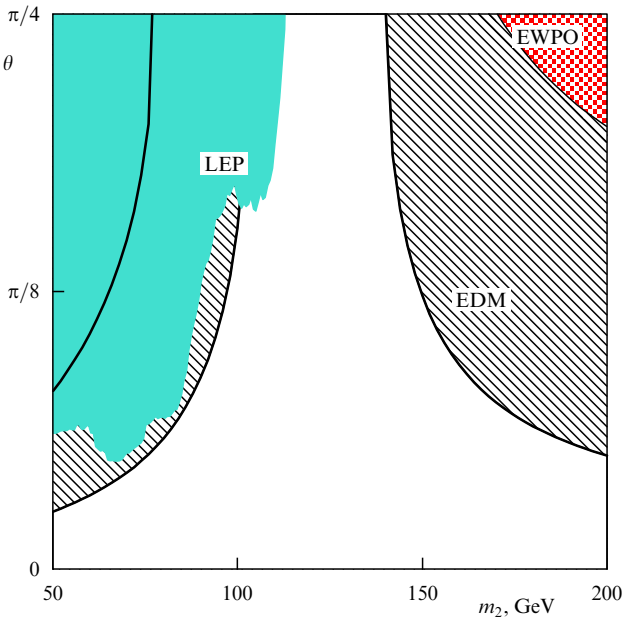

Figure 7. Bounds on the mass m_2 of the mostly singlet mass eigenstate and the mixing angle θ. The mostly Higgs state has the mass $m_1 = 120$ GeV. The scale of the new physics is $\Lambda_{CP} = 500$ GeV. EWPO: electroweak precision observables. Plot adapted from [56].

[7] 5D realizations of the composite Higgs field require a slight tuning to make the electroweak scale and hence the Higgs vev small [70].

coupling of the singlet to the (non-top) fermions and on the mass of the singlet.

4.2.4 Summary. Electroweak baryogenesis can be very easily realized in singlet extensions of the SM with a low cutoff. Since efficient sources of *CP* violation are present with dimension-five operators, the cutoff scale can be slightly larger than in the case of its minimal cousin, $\Lambda <$ a few TeV. Also, collider bounds and low-energy probes can be easily avoided if the $\mathbf{Z}_2$ symmetry of the singlet sector is only weakly broken. This makes the model compatible with phenomenology and insensitive to EDM constraints. However, we must note that this is somewhat against the philosophy of electroweak baryogenesis, which has falsifiability at its core.

4.3 Two-Higgs-doublet model

In the two-Higgs-doublet (THD) model, all necessary ingredients of electroweak baryogenesis are present, even if only renormalizable operators are considered. The most general scalar potential is given by

$$\begin{aligned} V(\Phi_1,\Phi_2) = &-\mu_1^2\Phi_1^\dagger\Phi_1 - \mu_2^2\Phi_2^\dagger\Phi_2 - \mu_3^2\left[\exp(\mathrm{i}\alpha)\Phi_1^\dagger\Phi_2 + \mathrm{h.c.}\right] \\ &+\frac{1}{2}\lambda_1(\Phi_1^\dagger\Phi_1)^2 + \frac{1}{2}\lambda_2(\Phi_2^\dagger\Phi_2)^2 + \frac{1}{2}\lambda_3(\Phi_2^\dagger\Phi_2)(\Phi_1^\dagger\Phi_1) \\ &+\lambda_4|\Phi_1^\dagger\Phi_2|^2 + \frac{1}{2}\lambda_5\left((\Phi_1^\dagger\Phi_2)^2 + \mathrm{h.c.}\right). \end{aligned} \tag{104}$$

The potential contains two complex (potentially *CP*-violating) couplings $\mu_3\exp(\mathrm{i}\alpha)$ and λ_5. Following the conventions in [57], we choose λ_5 to be real, such that α parameterizes *CP* violation in the scalar sector. As we see in the next section, the complexity of the scalar potential is also high enough to provide a strong first-order phase transition.

4.3.1 Phase transition. In principle, there are two regimes in the parameter space with a strong first-order phase transition. The first one is similar to the case discussed in the singlet extension in Section 4.2. The phase transition again proceeds in two steps, but unlike in the singlet extension, this first phase transition already breaks the electroweak symmetry in the THD model. This implies that for viable electroweak baryogenesis, this first phase transition has to be a strongly first-order one, which is not so easily achieved. We dismiss this possibility of a two-stage phase transition in what follows.

The reason that the phase transition can be much stronger than in the SM is two-fold. The first is that both Higgs doublets acquire a vev after the phase transition, and the form of the potential implies that the ratio $\tan\beta$ of these two vevs,

$$\begin{aligned} &\langle\Phi_1\rangle = \left(0, h_1\exp(\mathrm{i}\Theta_1)\right), \quad \langle\Phi_2\rangle = \left(0, h_2\exp(\mathrm{i}\Theta_2)\right), \\ &\tan\beta \equiv \frac{h_1}{h_2}, \end{aligned} \tag{105}$$

is not constant during the phase transition. The potential in terms of the vev $\phi^2 = h_1^2 + h_2^2$ is hence not necessarily polynomial and eventually develops a barrier between the two minima at the critical temperature. The second reason is that the scalar potential has enough free parameters to decouple the Higgs mass from the quartic coupling, which in the SM are related as $m_\mathrm{h}^2 = 2\lambda\phi_0^2$. It is thus possible to obtain a strong phase transition from thermal cubic contributions to the effective potential and at the same time to satisfy the LEP bound $m_\mathrm{h} > 114$ GeV.

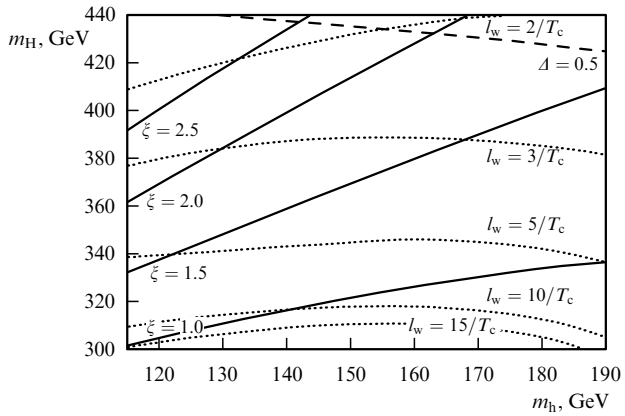

Figure 8. Lines of constant $\xi = \phi_\mathrm{c}/T_\mathrm{c}$ and l_w as a function of the two scalar masses m_h and m_H and for $\mu_3 = 100$ GeV and $\alpha = 0$ [μ_3 and α are respectively the coupling constant and the complex phase in potential (104)]. Δ is the line of the relative magnitude of one-loop corrections for the λ constants. Plot adapted from [57].

Overall, relatively strong phase transitions $\xi = \phi_\mathrm{c}/T_\mathrm{c} \gtrsim 1.5$, $l_\mathrm{w}T_\mathrm{c} \lesssim 10$ are possible for a Higgs mass above the LEP bound [57, 76–78]. Some examples are shown in Fig. 8.

4.3.2 Electroweak baryogenesis. The most general THD model with Yukawa couplings of fermions to both Higgs fields suffers from flavor-changing neutral currents already at the tree level. To avoid this problem, an additional $\mathbf{Z}_2$ symmetry is usually invoked that allows coupling the fermions to only one of the two doublets,

$$\Phi_1 \to -\Phi_1, \qquad \mathrm{d} \to \pm\mathrm{d}, \tag{106}$$

where, depending on the sign in the down sector, type I and type II THD models result. We note that the complex phase α in potential (104) breaks this symmetry explicitly, and therefore electroweak baryogenesis is not possible if this symmetry is also imposed on the scalar sector.

As before, the main source of baryogenesis comes from the top sector, and the corresponding Yukawa coupling has the form

$$\mathcal{L} \ni y_\mathrm{t}\bar{Q}_3\Phi_2 t. \tag{107}$$

The *CP*-violating source in this model comes not from the interplay of two operators that both contribute to the top mass but from the change of the complex phase Θ_2 in the Higgs field that couples to the top quark:

$$m_\mathrm{t} = \frac{y_\mathrm{t}}{\sqrt{2}}h_2\exp(\mathrm{i}\Theta_2). \tag{108}$$

The change in Θ_2 during the phase transition is induced by the dependence of the scalar potential on the relative phase $\Delta\Theta = (\Theta_1 - \Theta_2)/2$ that arises in the contributions involving α.

In [57], a part of the parameter space of the THD model is analyzed under the assumption that $\tan\beta$ does not change during the phase transition. However, using this assumption can lead to over-estimating the present *CP* violation, as is detailed in [79]. The reason is as follows: in the effective action for the vevs, the kinetic terms of the Higgs fields coming from

the phases yield the contributions

$$S \ni \frac{1}{2}(\Theta_1')^2 h_1^2 + \frac{1}{2}(\Theta_2')^2 h_2^2 = \frac{1}{2}(\Theta')^2 (h_1^2 + h_2^2) + \frac{1}{2}(\Delta\Theta')^2 (h_1^2 + h_2^2) + \Delta\Theta'\Theta' (h_1^2 - h_2^2)\,, \quad (109)$$

where we define the average phase $\Theta = (\Theta_1 + \Theta_2)/2$ and the relative phase $\Delta\Theta = (\Theta_1 - \Theta_2)/2$. Since the effective potential does not depend on the average phase Θ, we find (using the equations of motion)

$$\Theta' = -\frac{h_1^2 - h_2^2}{h_1^2 + h_2^2}\,\Delta\Theta'\,. \quad (110)$$

Reinserting this into the kinetic term gives

$$S \ni (\Delta\Theta')^2\,\frac{h_1^2 h_2^2}{h_1^2 + h_2^2}\,, \quad (111)$$

and for the individual phases,

$$\Theta_1' = \frac{2h_2^2}{h_1^2 + h_2^2}\,\Delta\Theta'\,, \qquad \Theta_2' = \frac{-2h_1^2}{h_1^2 + h_2^2}\,\Delta\Theta'\,. \quad (112)$$

It hence follows that *CP* violation in the top sector vanishes if one of the vevs vanishes on the trajectory during the phase transition (for $h_2 = 0$, the top mass vanishes, while for $h_1 = 0$, the phase Θ_2 is constant and no semiclassical force is present). On the other hand, we can always choose a basis where only one of the Higgs fields has a vev in the broken phase. If a constant $\tan\beta$ was imposed in this basis, *CP* violation would be absent. Therefore, the assumption of constant $\tan\beta$ is not only a basis-dependent statement but also of major importance for *CP* violation. Furthermore, this argument shows that the baryon asymmetry should be suppressed in the limit of very large or very small $\tan\beta$.

Numerically, study [57] found that a baryon asymmetry a few times larger than the observed one is possible in this setup. By contrast, the analysis in [79] additionally implemented (very strict) constraints on $Z \to b\bar{b}$ and generically found a smaller baryon asymmetry.

4.3.3 Collider and low-energy probes of the model. The THD model and its collider phenomenology are widely studied in the literature (see [80] for a recent review). In the context of electroweak baryogenesis, the main signatures are again the electron and neutron EDMs, but also the masses of the additional Higgs bosons, which have a large impact on the strength of the electroweak phase transition.

In agreement with [57], study [76] found that for a fixed Higgs mass m_h, stronger phase transitions can be obtained, especially if the additional Higgs bosons are rather heavy. As explained in [57], this arises from the fact that the larger masses stem from larger quartic couplings and, hence, it does not correspond to a decoupling of the additional Higgs bosons. On the other hand, the quartic couplings are not so essential for collider searches and EDM constraints, and therefore electroweak baryogenesis is rather unconstrained in this limit in the THD model. The limiting factor in this regime is the requirement that the perturbativity of the quartic couplings be preserved.

As mentioned above, additional constraints come from $Z \to b\bar{b}$. The main deviation from the SM stems from the loop contributions of the charged Higgs bosons to this process. In general, this drives the model to larger masses of the charged Higgs bosons and to larger $\tan\beta$. This is problematic for electroweak baryogenesis, since large values of $\tan\beta$ suppress the *CP*-violating semiclassical force. In [79], very strict bounds on this process (66% C.L.) have been implemented, which has a large impact on the final baryon asymmetry. If this constraint is treated more permissively (e.g., with 95% C.L.), the corresponding bound is not so relevant, and $\tan\beta$ is relatively unconstrained.

4.3.4 Summary. Electroweak baryogenesis is a viable option in the THD model. Without tuning the model, it allows a strong first-order phase transition and sufficient *CP* violation in the scalar sector, consistent with EDMs and collider probes. The main disadvantage of the model is that it does not have many benefits beyond electroweak baryogenesis. In particular, the hierarchy problem remains unsolved, and flavor issues cannot be solved by a discrete symmetry in those cases where electroweak baryogenesis is possible.

Overall, an improvement in the measurement of the neutron EDM by a factor of around ten can exclude electroweak baryogenesis in the THD model.

4.4 Minimal supersymmetric standard model

The minimal supersymmetric standard model (MSSM) is one of the most widely studied models today and one of the biggest contenders for resolving the question of how the large hierarchy between the electroweak and the Planck scales can be explained.

In the MSSM, the analysis of electroweak baryogenesis is very different from that in other models. First of all, there is no *CP* violation in the scalar potential or the top sector (beyond the Cabibbo–Kobayashi–Maskawa (CKM) *CP* violation of the SM), and hence the *CP* violation has to arise from a different source than in the cases discussed so far. In addition, it is not easy to obtain a strongly first-order phase transition in this setup. In particular, the ratio ϕ_c/T_c, even in the most optimistic scenarios, barely fulfills the wash-out bound (86), and the wall thickness is rather large, $l_w T_c \simeq 20$. This leads to a situation where the semiclassical force falls short in explaining the observed baryon asymmetry. Hence, electroweak baryogenesis in the MSSM has to be based on a different source of *CP* violation, e.g., the mixing between different charginos (and eventually neutralinos), which can be resonantly enhanced. A more extensive recent review of electroweak baryogenesis in the MSSM is given in Ref. [81], and we just present a short overview of the main points here.

4.4.1 Phase transition. The scalar potential in the MSSM is much more constrained than the one in the general THD model. At the tree level, it is given by

$$V_0 = m_1^2 h_1^2 + m_2^2 h_2^2 + 2m_3^2 h_1 h_2 + \frac{g^2 + g'^2}{8}(h_1^2 - h_2^2)^2\,. \quad (113)$$

With this potential, the mass of the lightest Higgs bosons is constrained to below the Z-boson mass. This is not compatible with the bounds from LEP and calls for large one-loop contributions to the Higgs mass:

$$V_1 = \sum_i \frac{n_i}{64\pi^2}\, m_i^4 \left(\log\frac{m_i^2}{Q^2} - \frac{3}{2}\right). \quad (114)$$

The dominant contributions to the Higgs mass come from the tops and stops that have Yukawa couplings of the order of unity and masses $m_t = y_t h_2$,

$$\mathcal{M}_{\tilde{t}}^2 = \begin{pmatrix} m_Q^2 + y_t^2 h_2^2 & y_t(A_t h_2 - \mu h_1) \\ y_t(A_t h_2 - \mu h_1) & m_U^2 + y_t^2 h_2^2 \end{pmatrix}, \tag{115}$$

where m_U, m_Q, and A_t are soft supersymmetry breaking terms, and μ stems from a term in the superpotential of the form $W \ni \mu H_1 H_2$. In order to obtain the Higgs mass $m_h \sim 125$ GeV, at least one of the stops has to be rather heavy: $m_{\tilde{t}_L} > 30$ TeV. This can be achieved by either a large soft mass m_Q or a large off-diagonal contribution from the A_t term.

The second option is not compatible with a strongly first-order phase transition, as we see in what follows. As in the SM, the potential barrier that is responsible for the first-order phase transition can only arise from thermal cubic terms in the effective potential (see Appendix D). Besides the degrees of freedom of the SM, only the stops can give such a sizable cubic term [82–86]. This means, in turn, that the right-handed stop (which is less constrained by electroweak precision tests than its left-handed partner) has to be very light. In particular, a cubic term is only delivered if the mixing between the stops is small and the thermal mass of the right-handed stop is countered by a negative soft mass, i.e.,

$$m_{\tilde{t}_R}^2(T) = m_U^2 + y_t^2 h_2^2 + \Pi(T)_{\tilde{t}_R} \simeq y_t^2 h_2^2 . \tag{116}$$

Additional constraints arise from the requirement that $\tan\beta$ not be too large and that the stop not develop a vev at low temperatures, which would lead to a spontaneous breaking of color. The results of this analysis from [87] are shown in Fig. 9. These results also have been qualitatively confirmed in lattice calculations [88].

4.4.2 Electroweak baryogenesis. As alluded to in Section 2.5, the determination of the baryon asymmetry in the MSSM is a controversial topic. One difference from the other models discussed so far is that *CP* violation does not arise in the top sector. The dominant source of *CP* violation turns out to be the charginos and neutralinos. For example, the chargino mass can be written as

$$\mathcal{M}_{\chi_\pm} = \begin{pmatrix} M_2 & g h_2 \\ g h_1 & \mu \end{pmatrix}, \tag{117}$$

where M_2 and μ can contain a complex phase.

This mass matrix leads to a semiclassical force source according to Eqn (50). But the phase transition in the MSSM is relatively weak [89, 90], $\phi_c/T_c \simeq 1$, $l_w T_c \simeq 20$, and therefore this source of *CP* violation is not sufficient to explain the observed baryon asymmetry once EDM constraints are imposed.

Hence, baryogenesis has to be driven by mixing effects in the MSSM. Parametrically, mixing effects are less suppressed, because they already appear in the first order in gradients, as can be seen in Eqn (50). The determination of the baryon asymmetry based on these mixing effects is to a certain extent still an open issue. The mass insertion formalism yields very large baryon asymmetry [41] but suffers from conceptual problems (see Section 2.6). Part of these problems can be overcome by resumming Higgs insertions [42], but some issues concerning finiteness of the results and how transport is established also remain in this framework. Conceptually, the cleanest way to tackle this problem is to use the first-principle approach in the Kadanoff–Baym framework. This was done in the analysis in [24], which particularly highlighted the importance of flavor oscillations. But also in this study, many simplifying assumptions were used. Namely, the coherent off-diagonal densities were assumed to be small. In particular, all contributions that are nominally of the second order in gradients were neglected. Whether these contributions are actually small is not so clear, since resonant effects can become important when the oscillation length is close to the wall thickness [20]. At first glance, this resonance condition is only satisfied for MSSM charginos for rather hard modes (which are sparse in the plasma), but this does not guarantee that the resonance can greatly enhance the baryon asymmetry.

Nonetheless, there are also some features that are shared by all approaches. For example, the baryon asymmetry is suppressed when the charginos are not almost mass degenerate or have a mass much larger than the temperature. This is seen in Fig. 10, which shows the regions of viable baryogenesis as a function of the two chargino mass parameters. A selection of quantitative results of chargino-driven baryogenesis in the MSSM is collected in Table 1.

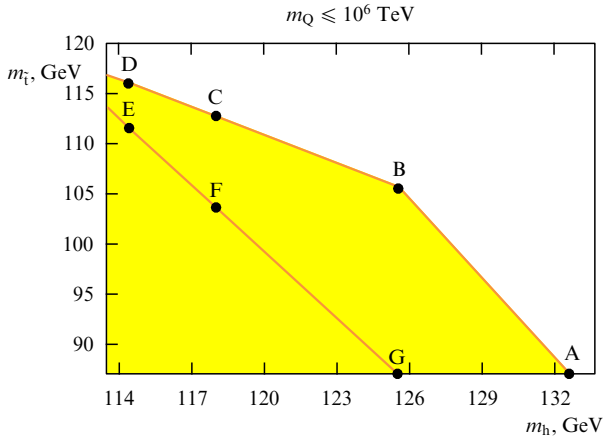

Figure 9. The window of a strong enough phase transition, $\phi_c/T_c > 1.0$, in the Higgs mass versus the light stop mass plane for the MSSM. A strong phase transition and the Higgs mass $m_h \simeq 125$ GeV can only be achieved at the cost of a very heavy left-handed stop, $m_Q \sim 10^6$ TeV. Plot adapted from [87].

Table 1. The largest possible baryon asymmetry for almost mass-degenerate charginos and a maximal *CP*-violating phase.

Method	η/η_{obs}	References
Mass insertion formalism; no Higgs resummation	~ 35	[41] (2000)
Mass insertion formalism; including Higgs resummation	~ 10	[42] (2002)
Mass insertion formalism; no Higgs resummation; more realistic diffusion network	~ 140	[43] (2004)
Kadanoff–Baym formalism; flavor oscillations; the adiabatic regime assumed	~ 3.5	[24] (2005)

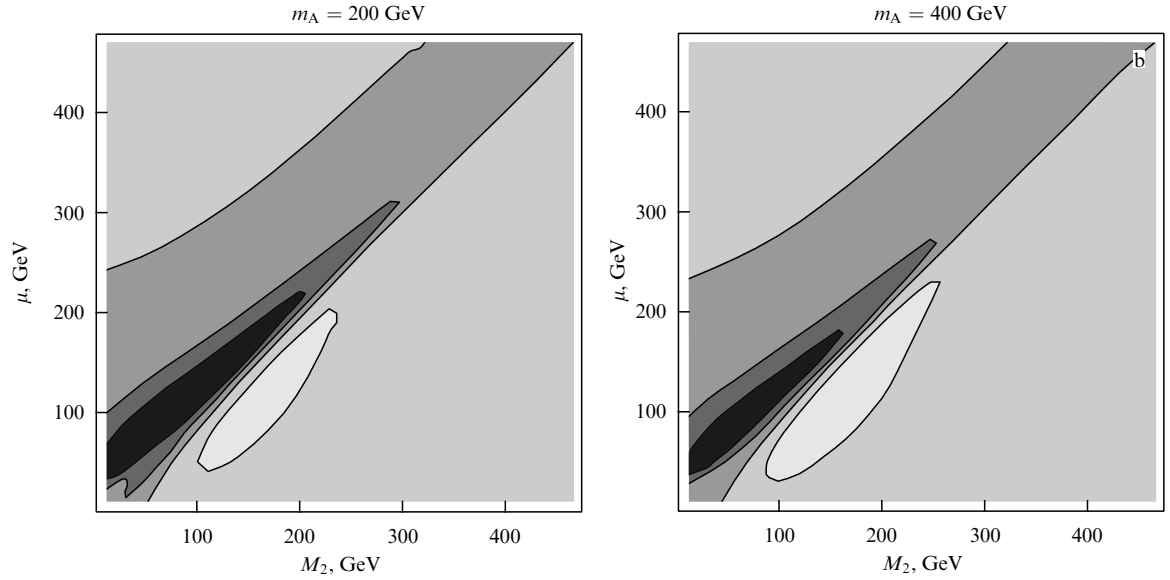

Figure 10. Contours of the regions with viable baryogenesis as a function of the two chargino mass parameters M_2 and μ. In the black region, the baryon asymmetry is larger than observed. Plot adapted from [24].

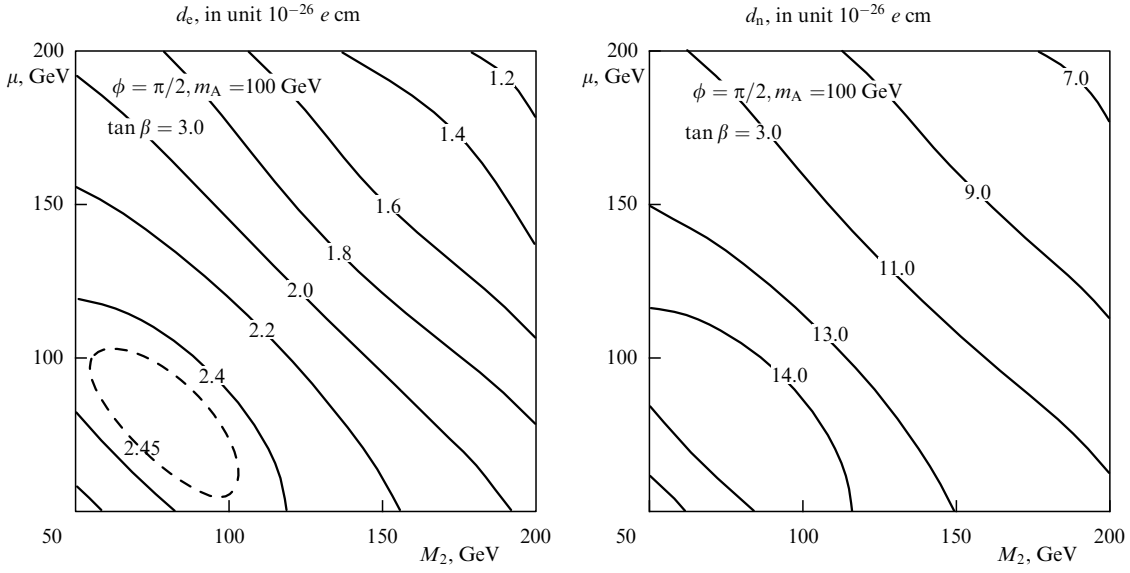

Figure 11. Contours of electron and neutron EDMs as functions of the two chargino mass parameters and for a maximal *CP* phase. Plot adapted from [93].

Beyond theses studies, neutralino [91] or stop-driven [92] baryogenesis has been considered for the MSSM in the literature. Neutralinos have the advantage that they do not suffer from EDM constraints as much as charginos do, but at the same time are somewhat less efficient in producing baryon asymmetry [91].

4.4.3 Collider and low-energy probes of the model. In the context of electroweak baryogenesis, the MSSM provides some special signatures. The first class of signals comes from the new source of *CP* violation in the chargino sector. Since the charginos cannot be much heavier than the electroweak scale in electroweak baryogenesis, this leads to sizable Barr–Zee contributions to the neutron and electron EDMs that can already be in conflict with experimental bounds. Furthermore, the dependence of the electron EDM on $\tan\beta$ and the chargino masses is quite similar to the dependence of the baryon asymmetry [93–95] (Fig. 11). This implies that the complex phase in the chargino sector cannot be larger than $\arg(\mu^* M_2) \lesssim 0.05$. This excludes chargino-driven electroweak baryogenesis in the MSSM in the most conservative approaches (see Table 1).

The second class of constraints is related to the requirement of a strong first-order phase transition. The most severe is the occurrence of stops close to the LEP bound [96–98]. Recent direct searches at the LHC are sensitive to light stops, and therefore this is only viable if stop decays are concealed through neutralino states with similar masses or some alternative mechanism [87]. Still, the light stops would have a large impact on the Higgs search.

Notably, they increase the loop-induced Higgs production rate by gluon fusion by a factor of 2 to 3. Moreover, light stops lead to a reduced branching ratio for the Higgs to diphotons due to a destructive interference with the dominant W-boson loop. Overall, light stops lead to an enhancement of the rate $gg \to H \to VV$ and a slight reduction in the rate $gg \to H \to \gamma\gamma$ compared to the SM. This produces a tension with the current data from Higgs searches [99–101], which can be partially relaxed by further assumptions about the particle spectrum [87].

4.4.4 Summary. Electroweak baryogenesis in the MSSM is an appealing scenario because the MSSM is the minimal setup that solves the hierarchy problem in a perturbative framework. The Higgs mass $m_h \sim 125$ GeV produces a tension with minimal supersymmetric models, particularly when a strongly first-order phase transition is demanded. In addition, this requires very light stops right above the LEP bound. That these states have been missed at the LHC so far is possible, but only if the particles that appear in the decay chain of the stops have peculiar masses [87]. The EDM constraints are also generically in conflict with chargino-driven electroweak baryogenesis. Hence, either other sources of *CP* violation (e.g., neutralinos) have to be used or the EDMs are small because of a cancellation of different contributions.

In summary, there remains a region of the parameter space in the MSSM in which electroweak baryogenesis is still viable. However, this possibility appears rather contrived, with several requirements arising in different sectors. The most constraining requirements can be traced back to the fact that Higgs masses $m_h \sim 125$ GeV are not easily realized in the MSSM. In extensions of the MSSM where the Higgs mass is achieved more naturally, the prospects of electroweak baryogenesis are much better. This is explicitly seen in the next model.

4.5 Next-to-MSSM

The main aim of singlet extensions of the MSSM is twofold. First, the μ-problem of the MSSM is solved. This is accomplished by adding a term $\lambda S H_1 H_2$ to the superpotential. When the singlet acquires a vev by spontaneous symmetry breaking, this operator produces an effective μ term. Second, additional contributions to the lightest Higgs mass improve the consistency with the current collider constraints. In what follows, we discuss a variant with only a trilinear coupling to the Higgs bosons and a linear term for the singlet in the superpotential, as was done in [102–104]. More general models can lead to new phenomena, such as transitional *CP* violation [106].

4.5.1 Phase transition. In this model, the scalar potential is given by

$$V_0 = m_1^2 h_1^2 + m_2^2 h_2^2 + 2m_3^2 h_1 h_2 + \frac{g^2 + g'^2}{8}(h_1^2 - h_2^2)^2 + m_s^2 s^2 + \frac{\lambda}{4} h_1^2 h_2^2 + a_\lambda s h_1 h_2 + t_s s \exp(\mathrm{i}\Theta_s) + \text{h.c.}, \quad (118)$$

where we define the scalar field vev as $\langle S \rangle = s \exp(\mathrm{i}\Theta_s)/\sqrt{2}$. Here, the parameter λ results from the term $\lambda S H_1 H_2$ in the superpotential, and t_s and a_λ are soft supersymmetry-breaking terms. Of special importance is the contribution $\lambda h_1^2 h_2^2/4$, which lifts the D-flat direction of the MSSM and can make a sizable contribution to the lightest Higgs mass.

The phase transition can become strong due to the interplay of the singlet and Higgs vevs and does not rely on thermal loop corrections. Already at the tree level, the model develops a first-order phase transition when [103]

$$m_s^2 < \frac{1}{\tilde{\lambda}} \left| \frac{\lambda^2 t_s}{m_s} - \frac{\sin(2\beta)}{2} m_s a_\lambda \right|, \quad (119)$$

where we define

$$\tilde{\lambda}^2 \equiv \frac{\lambda^2}{4} \sin^2(2\beta) + \frac{g^2 + g'^2}{8} \cos^2(2\beta). \quad (120)$$

For moderate values of λ, Higgs masses of the order of $m_h \sim 125$ GeV are possible and consistent with a strong phase transition. However, the parameter λ eventually develops a Landau pole at scales that are not too high, which implies the rough bound $\lambda < 0.7$.

4.5.2 Electroweak baryogenesis. Electroweak baryogenesis is easier to realize in the NMSSM (Next-to-Minimal Supersymmetric Standard Model) than in the MSSM for several reasons. First of all, the phase transition can be much stronger. This makes a considerable enhancement in the *CP*-violating source, which is very sensitive to ϕ_c/T_c, but also due to a reduced wall thickness. Furthermore, additional complex phases in the parameters t_s and a_λ lead to new sources of *CP* violation. In particular, the phases of the singlet and the Higgs fields change during the phase transition [104, 107]. The former leads to an additional semiclassical source in the chargino sector via the modified chargino mass matrix

$$\mathcal{M}_{\chi_\pm} = \begin{pmatrix} M_2 & g h_2 \exp(\mathrm{i}\Theta_2) \\ g h_1 \exp(\mathrm{i}\Theta_1) & -\lambda s \exp(\mathrm{i}\Theta_s) \end{pmatrix}, \quad (121)$$

as well as to a source in the top sector due to a change in Θ_2 during the phase transition. These contributions arise in the semiclassical force approach and do not rely on mixing. Additional sources by mixing can be as large as in the MSSM, but since the semiclassical forces do not require almost-mass-degenerate charginos, these contributions are typically much smaller. This allows a rather reliable determination of the baryon asymmetry, in contrast to the MSSM.

4.5.3 Collider and low-energy probes of the model. Compared to the MSSM, collider and EDM constraints are easier to satisfy in the NMSSM. As mentioned above, the lightest Higgs can obtain sizable mass contributions from the coupling to the singlet. But Higgs masses $m_h \sim 125$ GeV that rely solely on this coupling lead to a Landau pole in the coupling λ below the GUT scale. Hence, loop corrections from the stops and tops still have to be sizable, and stops heavier than a TeV are required. We note that light right-handed stops are not essential for a first-order phase transition, and they can therefore have masses similar to their left-handed counterparts.

Constraints from EDM measurements are also easier to avoid than in the MSSM. One reason is that the complex phase in the effective μ parameter is dynamic. Hence, it is possible that the phase is relatively small in the broken phase,

even though it varied significantly during the phase transition. Also, due to the stronger phase transition, electroweak baryogenesis is more efficient, and the observed baryon asymmetry can be reproduced with smaller complex phases in the chargino sector.

4.5.4 Summary. In a probabilistic study, the collider and mass constraints provide quite strong bounds on the parameters of the scalar sector. However, once these constraints are satisfied, a large portion of the remaining parameter space leads to a strong first-order phase transition and viable baryogenesis in the NMSSM [104]. In this sense, electroweak baryogenesis is a generic feature of the NMSSM.

4.6 Other models

For completeness, we briefly mention other models in which electroweak baryogenesis has been studied. This includes the Beyond-MSSM scenario [108, 109], the MSSM with an additional $\mathrm{U}(1)'$ gauge interaction [110–112], models with R-symmetric supersymmetry [113, 114], the singlet Majoron model [115], and left–right symmetric models [116].

5. Conclusions

The main ingredients of electroweak baryogenesis are a strong first-order phase transition and new sources of *CP* violation. For this reason, electroweak baryogenesis is ruled out in the SM and heavily constrained in the MSSM. Nevertheless, in models with a more general scalar sector, a strong first-order phase transition and electroweak baryogenesis are quite common features.

From the perspective of electroweak baryogenesis, these models have the added benefit that the determination of the baryon asymmetry is much more robust than in the MSSM. In most of these models, the dominant source of *CP* violation arises from a semiclassical force that is sensitive to the spin of a single particle species. By contrast, in the MSSM, the *CP* violation operative during the phase transition arises from flavor mixing in the chargino, neutralino, or stop sectors. This complicates the analysis through issues that are specific to systems with several flavors, such as flavor oscillations and resonant enhancements.

Ultimately, whether electroweak baryogenesis is a realistic scenario hinges on the questions of whether and how the hierarchy problem is solved by the new physics on the electroweak scale. The LHC discovery of a Higgs-like particle of the mass $m = 125$ GeV indicates that the MSSM can only solve the hierarchy problem at the cost of introducing a small hierarchy problem. This makes models with extended scalar sectors very attractive and, in turn, electroweak baryogenesis a promising mechanism for explaining the observed baryon asymmetry of the Universe.

Acknowledgments

It is a pleasure to thank my collaborators that worked with me on electroweak baryogenesis and related topics, in particular Stephan Huber, Tomislav Prokopec, and Michael G Schmidt. I would also like to thank Valery Rubakov for motivating me to write this review and Mathias Garny for carefully reading the manuscript and helpful suggestions. Finally, I would like to thank the corresponding authors for their permission to reproduce figures.

6. Appendices

A. Weak sphaleron rate

One essential ingredient of electroweak baryogenesis is the weak sphaleron rate.[8] It couples to left-handed fermions and antifermions of the SM and equally violates lepton and baryon number. In the presence of an (eventually local) *CP*-asymmetry in the left-handed particle densities, the sphaleron is biased toward a net baryon number. At the same time, any pre-existing baryon number diffuses as long as the baryon minus lepton number is conserved, $B = L$. The baryon asymmetry obeys the equation [29]

$$v_\mathrm{w} \frac{\mathrm{d}n_\mathrm{B}}{\mathrm{d}z} = \frac{3}{2} \Gamma_\mathrm{ws} \left(\frac{\mu_\mathrm{L}}{T} - \frac{15}{2} \frac{n_\mathrm{B}}{T^3} \right), \tag{122}$$

where Γ_ws is the weak sphaleron diffusion rate and μ_L denotes the chemical potential of the left-handed fermions. The final baryon asymmetry is then given by the integral

$$\eta = \frac{n_\mathrm{B}}{s} = \frac{405 \Gamma_\mathrm{ws}}{4\pi^2 v_\mathrm{w} g_* T^4} \int_0^\infty \mathrm{d}z \, \mu_\mathrm{L} \exp(-\nu z), \tag{123}$$

with $g_* \simeq 106.75$ being the effective number of degrees of freedom at electroweak temperatures and $\nu \equiv 45\Gamma_\mathrm{ws}/4v_\mathrm{w}T^3$. The chemical potential μ_L falls off at least as $\exp(-D_\mathrm{q} z)$ in the symmetric phase, where D_q is the quark diffusion constant. Thus, for high wall velocities v_w, the exponent $-\nu z$ is irrelevant and the dependence on the wall velocity is inherited from the chemical potential μ_L, which is in the leading order linear in v_w. Hence, for $\nu \ll D_\mathrm{q}$ and $v_\mathrm{w} \ll 1$, the final baryon asymmetry depends only weakly on the wall velocity. If v_w approaches the speed of sound, $c_\mathrm{s} = 1/\sqrt{3}$, diffusion should become inefficient (which, however, is not correctly reproduced in the analysis in Section 3, which assumes small wall velocities). In the limit of very small wall velocities, the exponent becomes important and leads to further suppression. This indicates that the wall is so slow that the sphaleron is saturated. In this regime, back reactions on the left-handed chemical potential μ_L should not be neglected.

On the one hand, the sphaleron rate has to be large during the phase transition in the symmetric phase in front of the wall. The *CP* violation in the reflection of particles leads to a net *CP*-violating particle density in front of the wall. If this particle density carries a (positive) lepton or (negative) baryon number, the sphaleron process is biased toward a positive net baryon number. To produce a baryon asymmetry of the observed magnitude $\eta \simeq 10^{-10}$, the sphaleron process should be considerably larger than η in electroweak units.

This sphaleron rate in the symmetric phase has been controversially discussed for some time in the literature.[9] The main problem is that the sphaleron rate is nonperturbative due to the large occupation number of soft modes, but is also sensitive to the dynamics of hard modes in the plasma [119]. The system is successfully described by Bödeker's effective theory [120–122], which can be easily simulated on a lattice. In conclusion, the weak sphaleron rate in the symmetric phase is given by

$$\Gamma_\mathrm{ws} = \kappa \left(\frac{g_\mathrm{w}^2 T^2}{m_\mathrm{D}^2} \right) \alpha_\mathrm{w}^5 T^4, \tag{124}$$

[8] An early review on the sphaleron rate in the context of electroweak baryogenesis is given in [117].

[9] A nice summary of the status quo can be found in talk [118].

where $m_D^2 = (11/6) g_w^2 T^2$ is the Debye mass of the weak gauge fields and g_w is the gauge coupling of the weak interactions. Numerically, the coefficient κ is given by $\kappa \simeq 40$. Including the dynamics of the Higgs field slightly reduces this number, and we find [123]

$$\Gamma_{ws} \simeq 1.0 \times 10^{-6}\, T^4 . \tag{125}$$

This is, in theory, sufficiently fast for electroweak baryogenesis.

On the other hand, the sphaleron rate in the broken phase should be smaller than in the symmetric one. For equal sphaleron rates, no net baryon number would be generated during the phase transition, since the plasma in the bubble carries the opposite lepton and baryon number densities compared to the plasma in front of the wall. In fact, the sphaleron rate in the broken phase must be many orders of magnitude smaller than the rate in the symmetric phase. After the phase transition, the plasma components inside and outside the Higgs bubbles mingle again. Even though a net baryon (and equal lepton) number was generated during the phase transition, the real equilibrium state of the system is still $B = L = 0$. If the sphaleron process is still active after the phase transition, the system returns to this equilibrium in a time of the order of the Hubble scale. Hence, for electroweak baryogenesis to work, the sphaleron rate must be slow compared to the Hubble expansion.

The sphaleron rate in the broken phase is accessible to semiclassical analysis [124, 125] and is exponentially suppressed by the sphaleron energy:

$$\Gamma_{ws} \simeq T^4 \exp\left(-\frac{E_{sp}}{T}\right) . \tag{126}$$

The sphaleron energy is proportional to [124]

$$E_{sp} \simeq \frac{4\pi \phi_c}{g_w}\, \Xi , \tag{127}$$

and is numerically given by $\Xi \simeq 2.8$. If we require that the sphaleron rate be slow compared to the Hubble expansion, $\Gamma_{ws} \ll H T^3$, then [125–128]

$$\phi_c \gtrsim 1.1\, T_c . \tag{128}$$

This is the so-called sphaleron wash-out criterion.[10]

In addition, the sphaleron rate in the broken phase has been confirmed nonperturbatively on the lattice [131]. Recently, the first lattice calculations connecting the symmetric phase with the broken phase have been presented [132], confirming the picture developed in the two different phases in a unifying framework.

B. Semiclassical approach to phase transitions

The formalism to describe semiclassical tunneling was pioneered in condensed matter systems by Langer [133], in quantum field theory by Coleman [134, 135], and at finite temperatures by Linde [136]. A review of the topic can be found in [137].

In a tunneling problem, the effective potential has at least two local minima that constitute the different phases in which the physical system can reside. In what follows, we call these two phases symmetric (before the phase transition) and broken (after the phase transition), motivated by the electroweak phase transition (Fig. 12). In the semiclassical WKB approximation, the tunnel probability per volume and time is suppressed by the Euclidean action of the so-called tunneling bounce $\bar{\phi}$,

$$P \sim A \exp\left(-S(\bar{\phi})\right) , \tag{129}$$

derived from the effective action expanded in gradients,

$$S \simeq \int \mathrm{d}^4 x\, \frac{1}{2}\, \partial^\mu \phi\, \partial_\mu \phi + V(\phi) , \tag{130}$$

where $V(\phi)$ denotes the corresponding effective potential, which eventually depends on the temperature.

The coefficient A in (129) must, for dimensional reasons, satisfy the condition $A \sim T^4$. The phase transition occurs when the probability of nucleating a bubble of the broken phase is of the order of unity in the Hubble volume and time, leading to the condition

$$S \simeq \log \frac{A}{H^4} \simeq 140 . \tag{131}$$

At zero temperature, the bounce $\bar{\phi}$ is an O(4)-symmetric solution of the Euclidean equations of motion, while at a finite temperature, it is O(3) symmetric and periodic in imaginary time. The equations of motion are then given by

$$\frac{\mathrm{d}^2 \bar{\phi}}{\mathrm{d}\tau^2} + (d-1)\, \frac{\mathrm{d}\bar{\phi}}{\tau\, \mathrm{d}\tau} = -\frac{\mathrm{d}V}{\mathrm{d}\bar{\phi}} , \tag{132}$$

with $d = 4$ ($d = 3$) for tunneling at zero (finite) temperature. The boundary conditions are such that $\bar{\phi}$ initially rests close to the broken phase and asymptotically approaches the symmetric phase at a late 'time':

$$\bar{\phi}(0) \simeq \phi_b , \qquad \bar{\phi}'(0) = 0 , \qquad \bar{\phi}(\infty) = \phi_s . \tag{133}$$

In the limit of weak phase transitions, the thin-wall approximation applies [134]. In this case, the field $\bar{\phi}$ rests for a rather long time τ_R close to the broken phase and then quickly changes to the symmetric phase. Here, the tunnel action can be reexpressed in terms of the wall tension

$$\sigma = \int \mathrm{d}\phi\, \sqrt{2V(\phi)} \tag{134}$$

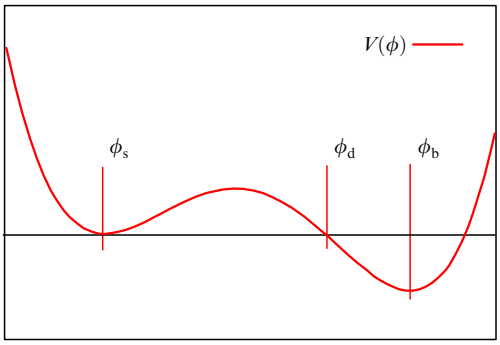

Figure 12. Example of a potential with a metastable minimum. The phase transition proceeds from the symmetric phase ϕ_s to the broken phase ϕ_b.

[10] For a more detailed discussion of this argument, see also [129, 130].

and the potential difference $\Delta V \equiv V(\phi_b) - V(\phi_s)$ as

$$S = \frac{27\pi^2\sigma^4}{2\Delta V^3}\,, \quad d=4\,, \qquad S = \frac{16\pi\sigma^3}{3T\Delta V^2}\,, \quad d=3\,. \tag{135}$$

Otherwise, for one field and quite arbitrary conditions, the tunneling action can easily be obtained numerically using the shooting algorithms [134]. For several scalar fields, more involved methods have to be used [138, 139].

Recently, the gauge independence of the above approach was questioned [129, 140, 141], but an explicit calculation in an Abelian toy model shows that the dependence on the gauge choice is actually quite small [142]. This is also supported by the fact that the semiclassical approach agrees reasonably well with nonperturbative methods on the lattice [143]. The main corrections to the above procedure seem to come from higher-order contributions to the kinetic term and the effective potential in effective action (130).

C. Wall velocity and wall thickness

Several parameters of the phase transition enter the produced baryon asymmetry quantitatively: the critical vev ϕ_c, the critical temperature T_c, the wall thickness l_w, and the wall velocity v_w.

The most important one is the ratio ϕ_c/T_c, which determines the sphaleron wash-out and also the reflection of particles by the Higgs wall, leading to *CP* violation in the particle densities. Fortunately, in most models with viable electroweak baryogenesis, these quantities can be rather easily obtained using the semiclassical methods of Appendix B. Another important input is the wall thickness l_w. The gradient expansion can only be applied for thick walls, $l_w T \gg 1$, and the final baryon asymmetry is in the one-flavor case roughly inversely proportional to the wall thickness. For wall velocities that are not too high, the shape of the Higgs bubble profile does not change much during expansion [144]. The wall thickness can then be determined from the wall thickness of the nucleated bubbles in the semiclassical tunneling analysis.

Finally, the wall velocity v_w enters the analysis. Viable baryogenesis requires that the wall velocity be small enough to allow particle diffusion in front of the wall, $v_w < 1/\sqrt{3}$. For wall velocities less than that, the produced baryon asymmetry is rather insensitive to the wall velocity, as was already discussed in Appendix A. This results from the fact that the *CP* violation accumulated in front of the wall is proportional to the wall velocity. At the same time, the phase transition proceeds longer and the sphaleron process can act longer on *CP*-violating particle densities and convert them into a baryon asymmetry. In this regime, the final baryon asymmetry depends only weakly on the wall velocity. However, for very slow walls, the sphaleron process becomes saturated, and the final asymmetry scales linearly with the wall velocity. Due to the smallness of the sphaleron rate, this typically happens for velocities $v_w \lesssim 10^{-3}$.

Therefore, the crucial question is whether the wall velocity is in the regime $10^{-3} \ll v_w < 1/\sqrt{3}$, where the above approximations are reasonable and the final asymmetry is insensitive to the wall velocity. Answering this question in a specific model requires performing an out-of-equilibrium analysis, which so far has only been performed in the SM [48, 145] and the MSSM [146]. In both cases, the wall velocity turned out to be in the desired vicinity. For other models, the wall velocity is still unknown. A simple way of estimating the wall velocity is to model friction in a phenomenological approach and to extrapolate the results from the SM and the MSSM [144, 147–150].

D. Electroweak phase transition in the Standard Model

In this section, we review the perturbative analysis of the electroweak phase transition in the SM. We follow study [151] but present a simplified analysis.

At the tree level, the effective potential of the Higgs field is

$$V^0 = \frac{\lambda}{4}(\phi^2 - v^2)^2\,, \tag{136}$$

and at the one-loop order, the thermal corrections to the free energy are

$$\Delta V^1 = \mp\frac{T^4}{2\pi^2}\sum_i \int \mathrm{d}x\, x^2 \log\left[1 \pm \exp\left(-\sqrt{x^2 + m_i^2\beta^2}\right)\right], \tag{137}$$

where $\pm$ respectively stand for fermions/bosons, T denotes the temperature, β is the inverse temperature, and m_i are the different particle masses. As long as the masses do not exceed the temperature, this can be expanded as

$$\Delta V^1_{\text{fermions}} = \frac{1}{48}\,m^2T^2 + O(m^4)\,, \qquad \Delta V^1_{\text{bosons}} = \frac{1}{24}\,m^2T^2 - \frac{1}{12\pi}\,m^3T + O(m^4)\,. \tag{138}$$

Of special importance are the cubic terms contributed by bosons. If the mass of a bosonic field is only generated by the coupling to the Higgs vev (as is the case for weak gauge bosons in the SM), this, in turn, gives rise to a term of the form $\phi^3 T$ in the effective potential. This term is essential to generate a potential barrier between the symmetric and the broken phase.

We consider a potential of the form

$$V = \mu^2(T)\phi^2 - ET\phi^3 + \frac{\lambda}{4}\,\phi^4\,. \tag{139}$$

At some temperature T_c, this polynomial potential has two degenerate minima at $\phi = 0$ and $\phi = \phi_c > 0$ and has the form

$$V = \frac{\lambda}{4}\,\phi^2(\phi - \phi_c)^2\,. \tag{140}$$

Comparison with (139) then shows that

$$\mu^2(T_c) = \frac{1}{4}\,\lambda\phi_c^2\,, \qquad ET_c = \frac{1}{2}\,\lambda\phi_c\,. \tag{141}$$

This immediately implies

$$\frac{\phi_c}{T_c} = \frac{2E}{\lambda}\,, \tag{142}$$

and larger Higgs masses lead to weaker phase transitions.

In the SM, the cubic coefficient arises only from the (transverse) electroweak gauge bosons [152–154], $E \sim 10^{-2}$. Accordingly, a phase transition strong enough for electroweak baryogenesis is only possible for Higgs masses below 40 GeV [155] in light of constraint (128). Moreover, for Higgs masses $m_h \gtrsim 70$ GeV, the perturbative analysis breaks down, and a crossover replaces the phase transition.

In the MSSM, additional contributions to the cubic term come from the right-handed stops when their mass is below the top mass. This can make the phase transition strong enough for baryogenesis in some parts of the parameter space, even when the Higgs mass $m_h \simeq 125$ GeV is assumed (see Section 4.4).

In general, if the potential barrier arises from a thermal cubic contribution, relation (142), in combination with the Higgs mass $m_h \simeq 125$ GeV, implies that a strong first-order phase transition requires $E \gtrsim 0.1$ at least. Thus, a moderate number of light bosons that couple strongly to the Higgs is essential in this case. Yet, in many models, the strength of the phase transition does not rely on thermal cubic contributions. The prime example of this is provided by models with an extended Higgs sector. When several scalar fields acquire a vev at electroweak scales, potential barriers can arise, even in the tree-level scalar potential (see Section 4.2).

References

1. Sakharov A D *JETP Lett.* **5** 24 (1967) [*Pis'ma Zh. Eksp. Teor. Fiz.* **5** 32 (1967)]
2. Kuzmin V A, Rubakov V A, Shaposhnikov M E *Phys. Lett. B* **155** 36 (1985)
3. Cohen A G, Kaplan D B, Nelson A E *Phys. Lett. B* **336** 41 (1994)
4. Schwinger J *J. Math. Phys.* **2** 407 (1961)
5. Keldysh L V *Sov. Phys. JETP* **20** 1018 (1965) [*Zh. Eksp. Teor. Fiz.* **47** 1515 (1964)]
   a. Keldysh L V "Real-time nonequilibrium Green's functions", in *Proc. of the Conf. Progress in Nonequilibrium Green's Functions II, 19 – 23 August 2002, Dresden, Germany* (Eds M Bonitz, D Semkat) (Singapore: World Scientific, 2003) p. 4
6. Kainulainen K et al. *JHEP* (06) 031 (2001)
7. Prokopec T, Schmidt M G, Weinstock S *Ann. Physics* **314** 208 (2004); hep-ph/0312110
8. Prokopec T, Schmidt M G, Weinstock S *Ann. Physics* **314** 267 (2004); hep-ph/0406140
9. Calzetta E, Hu B L *Phys. Rev. D* **37** 2878 (1988)
10. Berges J *AIP Conf. Proc.* **739** 3 (2004); hep-ph/0409233
11. Calzetta E A, Hu B-L B *Nonequilibrium Quantum Field Theory* (Cambridge: Cambridge Univ. Press, 2008)
12. Kapusta J I, Gale C *Finite-Temperature Field Theory. Principles and Applications* (Cambridge: Cambridge Univ. Press, 1989)
13. Bellac M L *Thermal Field Theory* (Cambridge: Cambridge Univ. Press, 1996)
14. Cornwall J M, Jackiw R, Tomboulis E *Phys. Rev. D* **10** 2428 (1974)
15. Danielewicz P *Ann. Physics* **152** 239 (1984)
16. Berges J *Phys. Rev. D* **70** 105010 (2004); hep-ph/0401172
17. Borsányi Sz, Reinosa U *Nucl. Phys. A* **820** 147c (2009); arXiv: 0810.4262
18. Garny M, Müller M M *Phys. Rev. D* **80** 085011 (2009); arXiv: 0904.3600
19. Kadanoff L P, Baym G *Quantum Statistical Mechanics. Green's Function Methods in Equilibrium and Nonequilibrium Problems* (New York: W.A. Benjamin, 1962)
20. Cirigliano V et al. *Phys. Rev. D* **81** 103503 (2010); arXiv:0912.3523
21. Kainulainen K et al. *Phys. Rev. D* **66** 043502 (2002); hep-ph/0202177
22. Konstandin T, Prokopec T, Schmidt M G *Nucl. Phys. B* **716** 373 (2005); hep-ph/0410135
23. Cirigliano V, Lee C, Tulin S *Phys. Rev. D* **84** 056006 (2011); arXiv: 1106.0747
24. Konstandin T et al. *Nucl. Phys. B* **738** 1 (2006); hep-ph/0505103
25. Joyce M, Prokopec T, Turok N *Phys. Rev. Lett.* **75** 1695 (1995); hep-ph/9408339
26. Joyce M, Prokopec T, Turok N *Phys. Rev. D* **53** 2930 (1996); hep-ph/9410281
27. Joyce M, Prokopec T, Turok N *Phys. Rev. D* **53** 2958 (1996); hep-ph/9410282
28. Joyce M, Prokopec T, Turok N *Phys. Lett. B* **339** 312 (1994)
29. Cline J M, Joyce M, Kainulainen K *Phys. Lett. B* **417** 79 (1998); hep-ph/9708393
30. Cline J M, Kainulainen K *Phys. Rev. Lett.* **85** 5519 (2000); hep-ph/0002272
31. Cline J M, Joyce M, Kainulainen K *JHEP* (07) 018 (2000); hep-ph/0006119
32. Cline J M, Joyce M, Kainulainen K, hep-ph/0110031
33. Huet P, Nelson A E *Phys. Lett. B* **355** 229 (1995); hep-ph/9504427
34. Huet P, Nelson A E *Phys. Rev. D* **53** 4578 (1996); hep-ph/9506477
35. Riotto A *Phys. Rev. D* **53** 5834 (1996); hep-ph/9510271
36. Carena M et al. *Nucl. Phys. B* **503** 387 (1997); hep-ph/9702409
37. Riotto A *Int. J. Mod. Phys. D* **7** 815 (1998); hep-ph/9709286
38. Riotto A *Nucl. Phys. B* **518** 339 (1998); hep-ph/9712221
39. Riotto A *Phys. Rev. D* **58** 095009 (1998); hep-ph/9803357
40. Rius N, Sanz V *Nucl. Phys. B* **570** 155 (2000); hep-ph/9907460
41. Carena M et al. *Nucl. Phys. B* **599** 158 (2001); hep-ph/0011055
42. Carena M et al. *Nucl. Phys. B* **650** 24 (2003); hep-ph/0208043
43. Lee C, Cirigliano V, Ramsey-Musolf M J *Phys. Rev. D* **71** 075010 (2005); hep-ph/0412354
44. Cirigliano V et al. *Phys. Rev. D* **73** 115009 (2006); hep-ph/0603058
45. Kainulainen K et al., hep-ph/0201245
46. Berges J *Nucl. Phys. A* **699** 847 (2002); hep-ph/0105311
47. Berges J, Borsányi Sz, Wetterich C *Phys. Rev. Lett.* **93** 142002 (2004); hep-ph/0403234
48. Moore G D, Prokopec T *Phys. Rev. D* **52** 7182 (1995); hep-ph/9506475
49. Fromme L, Huber S J *JHEP* (03) 049 (2007); hep-ph/0604159
50. Moore G D *Phys. Lett. B* **412** 359 (1997); hep-ph/9705248
51. Cline J M *Phys. Lett. B* **338** 263 (1994); hep-ph/9405365
52. Arnold P, Moore G D, Yaffe L G *JHEP* (11) 001 (2000); hep-ph/0010177
53. Arnold P, Moore G D, Yaffe L G *JHEP* (05) 051 (2003); hep-ph/0302165
54. Giudice G F, Shaposhnikov M *Phys. Lett. B* **326** 118 (1994); hep-ph/9311367
55. Bödeker D et al. *JHEP* (02) 026 (2005); hep-ph/0412366
56. Espinosa J R, Gripaios B, Konstandin T, Riva F *JCAP* (01) 012 (2012); arXiv:1110.2876
57. Fromme L, Huber S J, Seniuch M *JHEP* (11) 038 (2006); hep-ph/0605242
58. Elmfors P et al. *Phys. Lett. B* **452** 279 (1999); hep-ph/9809529
59. Chung D J H et al. *Phys. Rev. Lett.* **102** 061301 (2009); arXiv: 0808.1144
60. Chung D J H et al. *JHEP* (12) 067 (2009); arXiv:0908.2187
61. Chung D J H et al. *Phys. Rev. D* **81** 063506 (2010); arXiv:0905.4509
62. Kajantie K et al. *Phys. Rev. Lett.* **77** 2887 (1996); hep-ph/9605288
63. Hudson J J et al. *Nature* **473** 493 (2011)
64. Harris P G et al. *Phys. Rev. Lett.* **82** 904 (1999)
65. Grojean C, Servant G, Wells J D *Phys. Rev. D* **71** 036001 (2005); hep-ph/0407019
66. Delaunay C, Grojean C, Wells J D *JHEP* (04) 029 (2008); arXiv:0711.2511
67. D'Ambrosio G et al. *Nucl. Phys. B* **645** 155 (2002); hep-ph/0207036
68. Huber S J, Pospelov M, Ritz A *Phys. Rev. D* **75** 036006 (2007); hep-ph/0610003
69. Contino R, Nomura Y, Pomarol A *Nucl. Phys. B* **671** 148 (2003); hep-ph/0306259
70. Agashe K, Contino R, Pomarol A *Nucl. Phys. B* **719** 165 (2005); hep-ph/0412089
71. Agashe K et al. *Phys. Lett. B* **641** 62 (2006); hep-ph/0605341
72. Gripaios B et al. *JHEP* (04) 070 (2009); arXiv:0902.1483
73. Espinosa J R, Konstandin T, Riva F *Nucl. Phys. B* **854** 592 (2012); arXiv:1107.5441
74. Cline J M, Kainulainen K *JCAP* (01) 012 (2013); arXiv:1210.4196
75. Csáki C, Falkowski A, Weiler A *Phys. Rev. D* **80** 016001 (2009); arXiv:0806.3757
76. Cline J M, Kainulainen K, Vischer A P *Phys. Rev. D* **54** 2451 (1996); hep-ph/9506284

77. Cline J M, Lemieux P-A *Phys. Rev. D* **55** 3873 (1997); hep-ph/9609240
78. Cline J M, Kainulainen K *Phys. Rev. D* **87** 071701(R) (2013); arXiv:1302.2614
79. Cline J M, Kainulainen K, Trott M *JHEP* (11) 089 (2011); arXiv:1107.3559
80. Branco G C et al. *Phys. Rep.* **516** 1 (2012); arXiv:1106.0034
81. Morrissey D E, Ramsey-Musolf M J *New J. Phys.* **14** 125003 (2012); arXiv:1206.2942
82. Carena M S, Quirós M, Wagner C E M *Phys. Lett. B* **380** 81 (1996); hep-ph/9603420
83. Losada M *Nucl. Phys. B* **537** 3 (1999); hep-ph/9806519
84. Espinosa J R, Quirós M, Zwirner F *Phys. Lett. B* **307** 106 (1993); hep-ph/9303317
85. Carena M et al. *JHEP* (10) 062 (2008); arXiv:0806.4297
86. Carena M et al. *Nucl. Phys. B* **812** 243 (2009); arXiv:0809.3760
87. Carena M et al. *JHEP* (02) 001 (2013); arXiv:1207.6330
88. Cline J M, Kainulainen K *Nucl. Phys. B* **482** 73 (1996); hep-ph/9605235
89. Moreno J M, Quirós M, Seco M *Nucl. Phys. B* **526** 489 (1998); hep-ph/9801272
90. Huber S J, John P, Schmidt M G *Eur. Phys. J. C* **20** 695 (2001); hep-ph/0101249
91. Li Y, Profumo S, Ramsey-Musolf M *Phys. Lett. B* **673** 95 (2009); arXiv:0811.1987
92. Kozaczuk J et al. *Phys. Rev. D* **86** 096001 (2012); arXiv:1206.4100
93. Chang D, Chang W-F, Keung W-Y *Phys. Rev. D* **66** 116008 (2002); hep-ph/0205084
94. Pilaftsis A *Nucl. Phys. B* **644** 263 (2002); hep-ph/0207277
95. Cirigliano V et al. *JHEP* (01) 002 (2010); arXiv:0910.4589
96. Delepine D et al. *Phys. Lett. B* **386** 183 (1996); hep-ph/9604440
97. Cline J M, Moore G D *Phys. Rev. Lett.* **81** 3315 (1998); hep-ph/9806354
98. Balázs C, Carena M, Wagner C E M *Phys. Rev. D* **70** 015007 (2004); hep-ph/0403224
99. Menon A, Morrissey D E *Phys. Rev. D* **79** 115020 (2009); arXiv:0903.3038
100. Cohen T, Morrissey D E, Pierce A *Phys. Rev. D* **86** 013009 (2012); arXiv:1203.2924
101. Curtin D, Jaiswal P, Meade P *JHEP* (08) 005 (2012); arXiv:1203.2932
102. Panagiotakopoulos C, Pilaftsis A *Phys. Rev. D* **63** 055003 (2001); hep-ph/0008268
103. Menon A, Morrissey D E, Wagner C E M *Phys. Rev. D* **70** 035005 (2004); hep-ph/0404184
104. Huber S J, Konstandin T, Prokopec T, Schmidt M G *Nucl. Phys. B* **757** 172 (2006); hep-ph/0606298
105. Huber S J, Schmidt M G *Nucl. Phys. B* **606** 183 (2001); hep-ph/0003122
106. Kozaczuk J, Profumo S, Wainwright C L *Phys. Rev. D* **87** 075011 (2013); arXiv:1302.4781
107. Cheung K et al. *Phys. Lett. B* **710** 188 (2012); arXiv:1201.3781
108. Blum K, Nir Y *Phys. Rev. D* **78** 035005 (2008); arXiv:0805.0097
109. Blum K et al. *JHEP* (05) 101 (2010); arXiv:1003.2447
110. Kang J et al. *Phys. Rev. Lett.* **94** 061801 (2005); hep-ph/0402086
111. Ham S W, Oh S K *Phys. Rev. D* **76** 095018 (2007); arXiv:0708.1785
112. Kang J et al. *JHEP* (04) 097 (2011); arXiv:0911.2939
113. Kumar P, Pontón E *JHEP* (11) 037 (2011); arXiv:1107.1719
114. Fok R et al. *Phys. Rev. D* **87** 055018 (2013); arXiv:1208.2784
115. Cline J M et al. *JHEP* (07) 040 (2009); arXiv:0905.2559
116. Mohapatra R N, Zhang X *Phys. Rev. D* **46** 5331 (1992)
117. Rubakov V A, Shaposhnikov M E *Phys. Usp.* **39** 461 (1996) [*Usp. Fiz. Nauk* **166** 493 (1996)]; hep-ph/9603208
118. Moore G D, hep-ph/0009161
119. Arnold P, Son D, Yaffe L G *Phys. Rev. D* **55** 6264 (1997); hep-ph/9609481
120. Bödeker D *Phys. Lett. B* **426** 351 (1998); hep-ph/9801430
121. Bödeker D, Moore G D, Rummukainen K *Phys. Rev. D* **61** 056003 (2000); hep-ph/9907545
122. Bödeker D *Nucl. Phys. B* **559** 502 (1999); hep-ph/9905239
123. Moore G D *Phys. Rev. D* **62** 085011 (2000); hep-ph/0001216
124. Klinkhamer F R, Manton N S *Phys. Rev. D* **30** 2212 (1984)
125. Arnold P, McLerran L *Phys. Rev. D* **37** 1020 (1988)
126. Shaposhnikov M E *Nucl. Phys. B* **287** 757 (1987)
127. Shaposhnikov M E *Nucl. Phys. B* **299** 797 (1988)
128. Arnold P, McLerran L *Phys. Rev. D* **36** 581 (1987)
129. Patel H H, Ramsey-Musolf M J *JHEP* (07) 029 (2011); arXiv:1101.4665
130. Funakubo K, Senaha E *Phys. Rev. D* **79** 115024 (2009); arXiv:0905.2022
131. Moore G D *Phys. Rev. D* **59** 014503 (1999); hep-ph/9805264
132. D'Onofrio M, Rummukainen K, Tranberg A *JHEP* (08) 123 (2012); arXiv:1207.0685
133. Langer J S *Ann. Physics* **54** 258 (1969)
134. Coleman S *Phys. Rev. D* **15** 2929 (1977)
135. Callan C G (Jr.), Coleman S *Phys. Rev. D* **16** 1762 (1977)
136. Linde A D *Phys. Lett. B* **100** 37 (1981)
137. Quirós M *Helv. Phys. Acta* **67** 451 (1994)
138. Cline J M, Moore G D, Servant G *Phys. Rev. D* **60** 105035 (1999); hep-ph/9902220
139. Konstandin T, Huber S J *JCAP* (06) 021 (2006); hep-ph/0603081
140. Wainwright C, Profumo S, Ramsey-Musolf M J *Phys. Rev. D* **84** 023521 (2011); arXiv:1104.5487
141. Wainwright C L, Profumo S, Ramsey-Musolf M J *Phys. Rev. D* **86** 083537 (2012); arXiv:1204.5464
142. Garny M, Konstandin T *JHEP* (07) 189 (2012); arXiv:1205.3392
143. Moore G D, Rummukainen K *Phys. Rev. D* **63** 045002 (2001); hep-ph/0009132
144. Espinosa J R, Konstandin T, No J M, Servant G *JCAP* (06) 028 (2010); arXiv:1004.4187
145. Moore G, Prokopec T *Phys. Rev. Lett.* **75** 777 (1995); hep-ph/9503296
146. John P, Schmidt M G *Nucl. Phys. B* **598** 291 (2001); hep-ph/0002050
147. Mégevand A, Sánchez A D *Nucl. Phys. B* **820** 47 (2009); arXiv:0904.1753
148. Mégevand A, Sánchez A D *Nucl. Phys. B* **825** 151 (2010); arXiv:0908.3663
149. Huber S J, Sopena M *Phys. Rev. D* **85** 103507 (2012); arXiv:1112.1888
150. Huber S J, Sopena M, arXiv:1302.1044
151. Anderson G W, Hall L J *Phys. Rev. D* **45** 2685 (1992)
152. Carrington M E *Phys. Rev. D* **45** 2933 (1992)
153. Dine M et al. *Phys. Lett. B* **283** 319 (1992); hep-ph/9203201
154. Dine M et al. *Phys. Rev. D* **46** 550 (1992); hep-ph/9203203
155. Kajantie K et al. *Nucl. Phys. B* **466** 189 (1996); hep-lat/9510020